EVALUATION OF A NEW TURBULENCE MODEL FOR BOUNDARY LAYER FLOWS WITH PRESSURE GRADIENT

A THESIS SUBMITTED TO
THE GRADUATE SCHOOL OF NATURAL AND APPLIED SCIENCES
OF
MIDDLE EAST TECHNICAL UNIVERSITY

BY

ALP MARANGOZ

IN PARTIAL FULFILLMENT OF THE REQUIREMENTS

FOR

THE DEGREE OF MASTER OF SCIENCE

IN

AEROSPACE ENGINEERING

AUGUST 2005

Approval of the Graduate School of Natural and Applied Sciences.

Prof. Dr. Canan Özgen
Director

I certify that this thesis satisfies all the requirements as a thesis for the degree of Master of Science.

Prof. Dr. Nafiz Alemdaroğlu
Head of Department

This is to certify that we have read this thesis and that in our opinion it is fully adequate, in scope and quality, as a thesis for the degree of Master of Science.

Prof. Dr. Cahit Çıray
Supervisor

Examining Committee Members

Prof. Dr. Nafiz Alemdaroğlu

Prof. Dr. Cahit Çıray

Prof. Dr. Sinan Akmandor

Assoc. Dr. Sinan Eyi

Assoc. Dr. İsmail Aydın

I hereby declare that all information in this document has been obtained and presented in accordance with academic rules and ethical conduct. I also declare that, as required by these rules and conduct, I have fully cited and referenced all material and results that are not original to this work.

Alp MARANGOZ

ABSTRACT

EVALUATION OF A NEW TURBULENCE MODEL FOR BOUNDARY LAYER FLOWS WITH PRESSURE GRADIENT

Marangoz, Alp

M.S., Department of Aerospace Engineering

Supervisor: Prof. Dr. Cahit Çıray

August 2005, 103 pages

In this thesis, a new turbulence model developed previously for channel and flat plate flows is evaluated for flat plate flows with pressure gradient. For this purpose a flow solver, which uses boundary layer equations as the governing equations and Von Karman momentum integral equation for the calculation of skin friction, is developed.

It is shown that the error of the new turbulence model, in predicting the velocity profile, is less than 5 % for the flat plate flows without pressure gradient and less than 10 % for the flat plate flows with favorable pressure gradient. It is also shown that results with an error in the order of 20 % can be achieved for the

flat plate flows with adverse pressure gradient.

Keywords: Turbulence Modelling, Boundary Layer Flows

ÖZ

YENİ BİR TÜRBÜLANS MODELİNİN DEĞİŞKEN BASINÇLI SINIR TABAKA AKIMLARI İÇİN DEĞERLENDİRİLMESİ

Marangoz, Alp

Yüksek Lisans, Havacılık ve Uzay Mühendisliği Bölümü

Tez Yöneticisi: Prof. Dr. Cahit Çıray

Ağustos 2005, 103 sayfa

Bu tezde, daha önce kanal ve düz levha akımları için geliştirilen yeni bir türbülans modeli , değişken basınçlı düz levha akımları için değerlendirilmiştir. Bu amaçla, sınır tabaka denklemlerini çözen, duvar sürüklenmesini ise Von Karman momentum integral denklemi ile bulan, bir akım çözücü geliştirilmiştir.

Sabit basınçlı levha akımları için yeni türbülans modelinin hız hesaplamalarındaki hatanın % 5'den daha az olduğu ve negatif basınç değişimi altındaki levha akımları için hatanın ise % 10'dan daha iyi olduğu gösterilmiştir. Pozitif basınç değişimi altındaki levha akımları için ise hata seviyesi % 20'nin altında sonuçlar elde edilebileceği gösterilmiştir.

Anahtar Kelimeler: Türbülans Modellemesi, Sınır Tabaka Akımları

ACKNOWLEDGMENTS

First of all, I would like to thank my supervisor Prof. Dr. Cahit Çıray, not only for supervising my thesis but also for his support and encouragement during my masters education.

I am grateful to Dr. Sartuk Karasoy, my manager in Roketsan A.Ş. for allowing me to work on this thesis which was very important for me and my Chief Engineer Bülent Semerci, for his patience and understanding for the work hours I have spent for "turbulence", that I should have spent for "navigation".

I owe too much to the staff of the Roketsan Systems Engineering Department; Fatih, İlke, Ercan, Mine, Aylin, Barlas, Cenk abi, Osman abi, Sevil, Tolga, Cengizhan, Cemalettin and the others that I have forgot to mention. Each contributed to my education invaluably.

I would like to thank my cousin Emre and my friend Onur, for welcoming me in their houses and offices, where I used to spend my nights/days/hours working on this thesis.

Thank you Umut (for the backgammon!), Alper (for the booze!), Deniz (for the gossip!), Ufuk (for the support talks!), Murat (for the future plans!).

Thank you Soykan and Oğuz. Since our childhood, you cheered me up when-

ever I'm depressed and I hope you will continue all through my life.

Thank you Başak'cım. You were always there..

I owe too much to Ayça, who always told me what is right to do, although I have never listened.

Finally, I would like to thank to my family : I always felt your trust on me and I hope that you are and you will be proud of what I do in my life.

TABLE OF CONTENTS

LIST OF TABLES

TABLE

LIST OF FIGURES

FIGURES

LIST OF SYMBOLS

ROMAN SYMBOLS

c_p	Pressure coefficient [/]
H	Shape factor [/]
J	Jacobian of the transformation [/]
k	Specific turbulent kinetic energy [m^2/s^2]
k	Experimental constant for the New Model [/]
P	Pressure [Pa]
Re	Reynolds number (the subscript indicates the parameter on which Reynolds number based) [/]
U	Mean velocity component in x-direction (Streamwise direction) [m/s]
u_τ	Friction velocity [m/s]
U_e	The mean velocity at the edge of the boundary layer at a specific x location [m/s]
V	Mean velocity component in y-direction (Wall normal direction) [m/s]
W	Mean velocity component in z-direction [m/s]
x	Cartesian, spatial coordinate for streamwise direction [m]
y	Cartesian, spatial coordinate for wall normal direction [m]
z	Cartesian, spatial coordinate perpendicular to both x and y directions and together they form a right handed coordinate system. [m]

GREEK SYMBOLS

ξ	Transformed streamwise coordinate
η	Transformed wall normal coordinate
δ	Boundary layer thickness [m]
δ^*	Displacement thickness [m]
ν	Kinematic viscosity [m^2/s]
$\Re$	Set of Real Numbers
ρ	Density [kg/m^3]
∂	Partial derivative operator
ξ_x	Metric of transformation
η_y	Metric of transformation
τ	Shear stress [kg m^2/s^2]
θ	Momentum thickness [m]

SUBSCRIPTS

∞	Freestream value
T	Representing the turbulent quantities

SUPERSCRIPTS

j	Node index for x-direction
k	Node index for y-direction
$+$	Representing the wall units

Special Symbols

$\underline{A}$	Represents a vector quantity (A)
$\langle A \rangle$	Expected value, i.e. mean value of a quantity (A)
$\tilde{A}$	Represents a fluctuating component (A)
$\frac{DA}{Dt}$	Total derivative of a quantity (A)

CHAPTER 1

INTRODUCTION

1.1 Governing Equations of Fluid Motion

The equations that governs the fluid motion are the Navier-Stokes equations :

$$\frac{\partial \rho}{\partial t} + \frac{\partial \rho U}{\partial x} + \frac{\partial \rho V}{\partial y} + \frac{\partial \rho W}{\partial z} = 0$$

$$\begin{aligned}
\rho\frac{\partial U}{\partial t} + \rho U\frac{\partial U}{\partial x} + \rho V\frac{\partial U}{\partial y} + \rho W\frac{\partial U}{\partial z} &= -\frac{\partial P}{\partial x} + \frac{\partial}{\partial x}\left(\lambda \nabla \cdot \underline{V} + 2\mu\frac{\partial U}{\partial x}\right) \\
&+ \frac{\partial}{\partial y}\left[\mu\left(\frac{\partial V}{\partial x} + \frac{\partial U}{\partial y}\right)\right] + \frac{\partial}{\partial z}\left[\mu\left(\frac{\partial U}{\partial z} + \frac{\partial W}{\partial x}\right)\right] \\
\rho\frac{\partial V}{\partial t} + \rho U\frac{\partial V}{\partial x} + \rho V\frac{\partial V}{\partial y} + \rho W\frac{\partial V}{\partial z} &= -\frac{\partial P}{\partial y} + \frac{\partial}{\partial x}\left[\mu\left(\frac{\partial V}{\partial x} + \frac{\partial U}{\partial y}\right)\right] \\
&+ \frac{\partial}{\partial y}\left(\lambda \nabla \cdot \underline{V} + 2\mu\frac{\partial V}{\partial y}\right) + \frac{\partial}{\partial z}\left[\mu\left(\frac{\partial W}{\partial y} + \frac{\partial V}{\partial z}\right)\right] \\
\rho\frac{\partial W}{\partial t} + \rho U\frac{\partial W}{\partial x} + \rho V\frac{\partial W}{\partial y} + \rho W\frac{\partial W}{\partial z} &= -\frac{\partial P}{\partial z} + \frac{\partial}{\partial x}\left[\mu\left(\frac{\partial U}{\partial z} + \frac{\partial W}{\partial x}\right)\right] \\
&+ \frac{\partial}{\partial y}\left[\mu\left(\frac{\partial W}{\partial y} + \frac{\partial V}{\partial z}\right)\right] + \frac{\partial}{\partial z}\left(\lambda \nabla \cdot \underline{V} + 2\mu\frac{\partial W}{\partial z}\right)
\end{aligned} \tag{1.1}$$

where ∇ is the *divergence operator*, $\underline{V}$ is the *total velocity vector*, i.e. $\underline{V} = \begin{bmatrix} U & V & W \end{bmatrix}^T$,

μ is the *dynamic viscosity* and λ is the *bulk viscosity coefficient* which is hypothesized to be equal to $\lambda = -\frac{2}{3}\mu$.

A third relation for conservation of energy can be added to this system. Total of 5 equations represent the conservation equations of the classical physics : 1 for conservation of mass, 3 for conservation of linear momentum (in 3 directions) and 1 for conservation of energy. Actually the Navier-Stokes equations are nothing but the application of Newton's second law of motion ($F = m \cdot a$) to a control volume. The equations are derived independently by a French mathematician M. Navier and an English physicist G. Stokes in the first half of the nineteenth century ([2]). The derivation can be found in any standard textbook on fluid dynamics (for example [2]).

The Navier-Stokes equations are nonlinear partial differential equations and their analytical solution does not exist except for very special cases. Even its full numerical solution cannot be calculated unless the *Reynolds Number*, which is a nondirectional constant defined as,

$$Re = \frac{U \cdot l}{\nu}$$

where U is a characteristic velocity, l is a characteristic length scale and ν is the kinematic viscosity, is small. It represents the ratio of inertial forces to viscous forces from one point of view ([2]) and the ratio of largest scale of motion to the smallest scale, in another ([22]).

This nonlinear behavior of the Navier-Stokes equations led the scientist to divide the fluid dynamics problems to classes where some effects negligibly affect the parameters under interest. For example, for small Mach numbers ($M < 0.3$),

the variation of the density within the flow field can be assumed to be negligible and the derivative of density can be taken to be zero in the Navier-Stokes equations. Then it is said that the flow is incompressible and for incompressible and adiabatic flows, it is not necessary to use energy equation since it can be derived from the linear momentum equations. For the calculation of the lift around a body, viscosity has a small effect and it can be assumed to be zero and the Navier-Stokes equations results in Euler equations with this assumption. Likewise for the investigation of turbulent motion, some assumptions on the flow can be made.

The theoretical work on the viscous flow problem lead to widely used theories that further simplify the problem; The *Boundary Layer Theory* and the *Thin Shear Layer Assumption* which will be explained in the subsequent sections. But before going into these subjects, it is required to explain another important point in the approach to the turbulent flow problem.

1.2 Averaging

The first important step towards the revelation of turbulence is taken by Osborne Reynolds at the end of the nineteenth century. Reynolds proposed that for turbulent flows, Navier-Stokes equations are valid for instantaneous quantities, i.e. the exact value of the quantities at a specific time. However instantaneous quantities are difficult to deal with, due to the inherent stochastic nature of turbulence. To avoid this problem, he proposed that instantaneous value of a variable under the turbulent motion can be divided into two components : A mean value which is

time independent and a fluctuating component whose mean value is zero :

$$\underline{V} = \langle \underline{V} \rangle + \underline{\tilde{v}}$$

The mean value taken in different forms. For example, taking the average over a mass leads to Favre averaging or taking the average over time leads to Reynolds averaging. The averaging method strongly depends on the nature of the turbulent motion. Turbulent motion is inherently a stochastic process and there are some properties of stochastic processes which permit to make simplifications on the calculations, like stationarity, ergodicity etc. ([6]). For most of the engineering applications, time averaging is the appropriate way of representing the variables under turbulent motion ([30]).

The new variables (fluctuating and mean components) can be substituted in the The Navier-Stokes equations. After this substitution, if the time average of the both sides of the Navier-Stokes equations is taken; new set of equations can be generated. This new set of equations are called the Reynolds Averaged Navier-Stokes equations or in short, RANS equations. The RANS equations for incompressible flows, in indicial notation (with Einstein summation convention) is given in (1.2).

$$\frac{\partial \langle U_i \rangle}{\partial x_i} = 0$$

$$\frac{\partial \langle U_i \rangle}{\partial t} + \langle U_i \rangle \frac{\partial \langle U_i \rangle}{\partial x_j} = -\frac{1}{\rho}\frac{\partial P}{\partial x_j} + \frac{\partial}{\partial x_j}\left[\nu\left(\frac{\partial \langle U_i \rangle}{\partial x_j} + \frac{\partial \langle U_j \rangle}{\partial x_i}\right) - \langle \tilde{u}_i \tilde{u}_j \rangle\right] \qquad (1.2)$$

The last term at the right hand side of (1.2) is called the *Reynolds Stress Tensor*, which is a symmetric tensor and it brings six more unknowns to the fluid

flow problem. The equations for the components of the Reynolds Stress Tensor can be generated similar to the derivation of the RANS equations. However these new equations involve higher order correlations of the velocity, hence new unknowns to the problem. The procedure can be proceeded indefinitely and new unknowns will emerge ([30]). Therefore it is impossible to get a finite number of equations equal to the unknowns. This is called the *Closure Problem*.

With the use of (1.2) instead of original Navier-Stokes equations, the solution reduces to calculating the mean quantities instead of instantaneous quantities. However it is not in closed form (The Reynolds stress tensor should be calculated explicitly, which is actually the modelling of turbulence) and still it requires a heavy computational power.

1.3 Highlights of Boundary Layer Theory

Analytical solution of Navier-Stokes equations exists for some cases. However the solution of it for a general flow problem should be found numerically. Therefore further simplifications are sought. For this purpose, *Boundary Layer Theory* is proposed by Prandtl in 1904. With his own words, Prandtl explains the idea behind the boundary layer theory as :

> *A very satisfactory explanation of the physical process in the boundary layer between a fluid and a solid body could be obtained by the hypothesis of an adhesion of the fluid to the walls, that is, by the hypothesis of a zero relative velocity between fluid and wall. If the viscosity was very small and the fluid path along the wall not too long, the fluid velocity ought to resume its normal value at a very short distance from the wall. In the thin transition layer however, the sharp changes of velocity, even with small coefficient of friction, produce marked results.*
>
> Ludwig Prandtl, 1904 [1]

[1] This quotation is taken from [2]

This physical argument actually means that the fluid velocity changes from its zero value at the wall to the freestream value within a very narrow band therefore the gradient of the velocity ($\frac{\partial \langle U \rangle}{\partial y} \gg 0$) is very large which leads to large viscous stresses ($\tau = \mu \frac{\partial \langle U \rangle}{\partial y}$), in this region. As the freestream is approached, the gradient of the velocity becomes very small ($\frac{\partial \langle U \rangle}{\partial y} \ll 0$) and therefore viscous stresses are negligible at this outer part of the flow.

In the limiting case of $\lim_{\mu \to 0}$, $Re \to \infty$, and $\delta \ll L$, where δ is the boundary layer thickness and L is a characteristic length of the flow. For this condition, Navier-Stokes equations can be simplified to form boundary layer equations. Similarly, the RANS equations can be simplified to boundary layer equations valid for mean quantities. Two dimensional form of boundary layer equations is given in (1.3), ([24])

$$\begin{aligned} \frac{\partial \langle U \rangle}{\partial x} + \frac{\partial \langle V \rangle}{\partial y} &= 0 \\ \langle U \rangle \cdot \frac{\partial \langle U \rangle}{\partial x} + V \cdot \frac{\partial \langle U \rangle}{\partial y} &= -\frac{1}{\rho} \cdot \frac{dP}{dx} + \frac{1}{\rho} \cdot \frac{\partial}{\partial y} \left(\mu \frac{\partial^2 \langle U \rangle}{\partial y^2} - \langle \tilde{u} \tilde{v} \rangle \right) \end{aligned} \tag{1.3}$$

As can be seen from (1.3) and (1.2), the two linear momentum equations in (1.2) is reduced to a single equation in (1.3) (for 2D flows of course). In fact, the linear momentum equation in y direction reduces to the $\frac{\partial P}{\partial y} = 0$ condition which indicates that pressure does not change within the boundary layer. Therefore $P(y) = P(\delta)$ and $\frac{dP}{dx} = \frac{dP(y)}{dx} = \frac{dP(\delta)}{dx}$ which can be taken from an inviscid solution of the flowfield.

Boundary layer theory greatly simplifies the Navier-Stokes equations yet keeps its nonlinear character ([24]). However there are some limitations about the appli-

cability of the boundary layer equations. These can be summarized as following ([28]):

- The accuracy of the equations increases with increasing Reynolds number. Therefore it is not appropriate to use the theory for low Reynolds number regions.
- Not valid in separated flow regions
- Not valid at the trailing edge
- Not able to to predict the effect of strong wall curvature, whether transverse or longitudinal, but it can be applied to flows around airfoils
- Not able to predict the effect of finite shear (vorticity) in the outer stream

The appropriate boundary conditions are,

$$\langle U\rangle|_{y=0} = 0 \qquad \lim_{y\to\infty}\langle U\rangle = U_e \quad or \quad \lim_{y\to\infty}\frac{\partial\langle U\rangle}{\partial y} = 0$$

$$\langle V\rangle|_{y=0} = 0$$

In this thesis, the flowfield around a flatplate is solved using the boundary layer equations. The inner structure of the boundary layer and the solution techniques of the equations are explained in appropriate sections of Chapter 3.

Another approach to boundary layer equations is through perturbation techniques. For large value of Re, $1/Re$ becomes very small and this parameter can be used as a perturbation parameter. With this perturbation parameter, Navier-Stokes equations become a singular perturbation problem. This actually means that the perturbed solution of the equations is not the limit of the solution of

the unperturbed equation when the perturbation parameter approaches zero, i.e. the viscous solution of the Navier-Stokes equations is not the solution of Euler equations without viscosity (Refer to [7] for more information about the perturbation theory). The solution of the singular perturbation problem of Navier-Stokes equations leads to the boundary layer equations. The advantage of such an approach is that higher order perturbation equations can be derived, i.e. containing higher order μ terms. These higher order boundary layer equations ((1.3) is also called first order boundary layer equation) are said to compensate for some of the disadvantages of the first order boundary layer equations, mentioned previously ([24]).

1.4 Highlights of Thin Shear Layer Assumption

Thin shear layer assumption is another assumption set that permits to make simplification on the Navier-Stokes equations. It is proposed by Baldwin and Lomax in [5]. This assumption comes from the fact that in a flow inside a shear layer (The shear layer can be defined as the part of a flow in which shear stress interacts with a large cross-stream gradient of streamwise velocity), streamwise gradients of U, or of other quantities are very small compared with cross-stream gradients of the same quantity ([9]). This leads to neglecting of viscous derivatives in streamwise direction while retaining the terms in transverse direction ([21]). The thin shear layer assumption is similar to boundary layer theory but the normal linear momentum equation, which is neglected in the boundary layer theory, is also solved and the change of pressure within the shear layer is permitted. The

thin shear layer assumption can break down for low Reynolds numbers and in regions of massive flow separation ([21]).

Thin shear layer assumption is a less strict assumption than the boundary layer assumption. Hence it brings less simplification to the original Navier-Stokes equations. RANS solvers usually use this assumption to simplify the original Navier-Stokes equations.

1.5 Turbulence Modelling

1.5.1 Some Guides to Turbulence Models

By definition, turbulence is the random fluctuation in the properties of flow. However how this motion is sustained [2] is the key question in understanding the turbulence calculation techniques. This can be investigated through the energy equation of the mean flow (1.4) and the turbulent motion (1.5).

$$\begin{aligned}\frac{\partial\langle E\rangle}{\partial t}+\frac{\partial\langle U_j\rangle\langle E\rangle}{\partial x_j} &= -\frac{\partial}{\partial x_j}\left(\langle P\rangle\langle U_i\rangle\right)-\frac{\partial}{\partial x_j}\left(2\mu\langle S_{ij}\rangle\langle U_i\rangle\right) \\ &\quad -\frac{\partial}{\partial x_j}\left(\rho\langle\tilde{u}_i\tilde{u}_j\rangle\langle U_i\rangle\right)-2\mu\langle S_{ij}\rangle\langle S_{ij}\rangle+\rho\langle\tilde{u}_i\tilde{u}_j\rangle\frac{\partial\langle U_i\rangle}{\partial x_j}\end{aligned} \tag{1.4}$$

$$\begin{aligned}\frac{\partial\langle\tilde{e}\rangle}{\partial t}+\frac{\partial\langle U_j\rangle\langle\tilde{e}\rangle}{\partial x_j} &= -\frac{\partial\langle\tilde{P}p\tilde{u}_i\rangle}{\partial x_j}-\frac{\partial\langle\tilde{e}\tilde{u}_i\rangle}{\partial x_j}+\frac{\partial}{\partial x_j}\left(2\mu\langle\tilde{s}_{ij}\tilde{u}_i\rangle\right)-2\mu\langle\tilde{s}_{ij}\tilde{s}_{ij}\rangle \\ &\quad -\rho\langle\tilde{u}_i\tilde{u}_j\rangle\frac{\partial\langle U_i\rangle}{\partial x_j}\end{aligned} \tag{1.5}$$

where S_{ij} and $\tilde{s}_{ij}$ are the strain rates of mean flow and the turbulent motion,

[2] This questions does not direct to the problem that how a laminar flow becomes a turbulent flow since this is the topic of another area

respectively, i.e. ;

$$S_{ij} = \frac{1}{2}\left(\frac{\partial U_i}{\partial x_j} + \frac{\partial U_j}{\partial x_i}\right) \qquad \tilde{s}_{ij} = \frac{1}{2}\left(\frac{\partial \tilde{u}_i}{\partial x_j} + \frac{\partial \tilde{u}_j}{\partial x_i}\right)$$

These equations indicate that Reynolds stresses convey energy from the mean flow to the turbulent motion and turbulent motion dissipates energy by the strain correlation. In other words, the the energy is transferred from the larger eddies to the smaller eddies and the smallest eddies dissipate the energy. The situation is summarized in Figure 1.1.

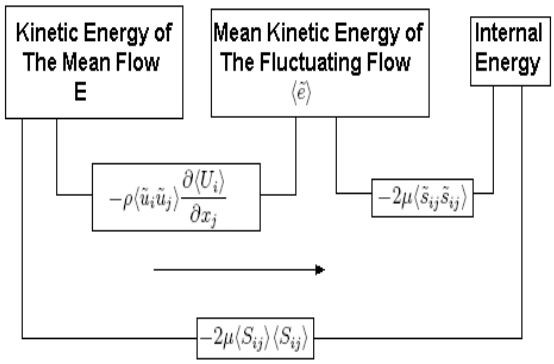

Figure 1.1: Energy transfer between the mean flow and the turbulent motion (Taken from [8])

It should be reminded that, in Figure 1.1, it is implied that the energy flow is unidirectional and it is for most of the cases. But in some complex flows, the reverse energy transfer can also be observed. It is realized by the change in the signs of the transfer terms ([8]).

The energy cascade is a very important phenomenon and when combined with Kolmogorov's hypotheses, it gives valuable insight about turbulence. Kolmogorov divides the energy spectrum of the turbulence in terms of the wavelength of the eddies. The largest eddies have a lengthscale (l_0) on the order of the lengthscale

of the flow (L). The smallest eddies are responsible for the dissipation and it is assumed that the smallest eddies are dissipated at one turn-over time. They have the lengthscale of η. With these definitions, Kolmogorov's hypotheses can be written as,

Kolmogorov's hypothesis of local isotropy. At sufficiently high Reynolds number, the small-scale turbulent motions ($l \ll l_0$) are statistically isotropic

Kolmogorov's first similarity hypothesis. In every turbulent flow at sufficiently high Reynolds number, the statistics of the small-scale motions ($l < l_{EI}$) have a universal form that is uniquely determined by ν and ε.

ν is the kinematic viscosity and ε is the dissipation rate. The range $l < l_{EI}$ is referred to as the *universal equilibrium range*.

Kolmogorov's second similarity hypothesis. In every turbulent flow at sufficiently high Reynolds number, the statistics of the motions of scale l in the range ($l_0 \gg l \gg \eta$ have a universal form that is uniquely determined by ε, independent of ν.

Then the energy spectrum can be divided into three : Energy Containing Range, Inertial Subrange and Dissipation Range which are shown in Figure 1.2. The important thing about this division is that the character of Inertial Subrange and Dissipation Range is universal.

Actually this energy spectrum is the key point to weight the turbulence modelling (or calculation) techniques, which will be described in the following sections.

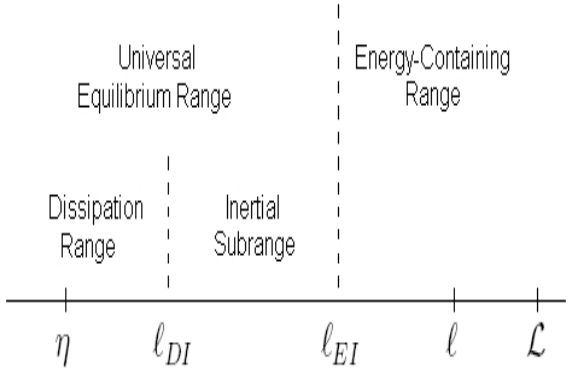

Figure 1.2: Ranges in the energy spectrum (Taken from [22])

1.5.2 Numerical Simulations

The simplest idea to approach the turbulent motion is to simulate [3] the Navier-Stokes equations within time numerically as can be done to any time dependent system of equations. Unfortunately, simple does not mean easy in most of the cases and numerical simulation of turbulent motion is not an exception. Indeed, it became possible only since 1970s, after the advent of supercomputers.

In order to numerically simulate the flow, the whole energy spectrum of the turbulent motion can be solved and every detailed information about the turbulence can be acquired. This approach is called the *Direct Numerical Simulation* or in short, *DNS*. However, this is a very difficult process. The turbulent motion involves very large and small scales of motion, from the length scale of the flow (L) to Kolmogorov scales (η), as described in section 1.5.1. This requires a very high resolution grid and a very very high speed computers in order the solve the equations. The computation time increases with $Re^{9/4}$ ([8]). With the current

[3] the word *Simulate* is used instead of *Solve* because the unsteady nature of turbulence requires a solution as an evolution of the flow from an initial state

state of supercomputers, it is only possible to make calculations on limited cases. The computations are restricted to rather low Reynolds Number flows and still the computation time is on the order of 200 hours ([8]). But the interest in DNS calculations does not come from an engineering point of view. Since DNS gives the whole character of the turbulent motion, it is very valuable in turbulence research. With DNS, it is possible to get direct information which are impossible to acquire from experiments.

The lengthy computation time makes DNS not practical for most of the flows under engineering interest. Kolmogorov's hypotheses come to help in this case. As explained in section 1.5.1, the small scale motions of turbulence are universal. Therefore, since most of the intellectual and computational work on DNS is concentrated to the simulation of small scale motions ([22]), it is a good idea to simulate numerically the large scale motions of turbulence, which are flow dependent, and model the small scale turbulent motions. This technique is called *Large Eddy Simulation* or in short, LES. For this purpose, the Navier-Stokes equations are written in frequency domain. The large scale motions (low frequency, High wavelength or *Large Eddies*) are handled in frequency domain while high frequency components are filtered and calculated using turbulence closures ([22]).

The cut off frequency between the large and small scale motions determine the type of the LES. For example if a large portion of the spectrum is filtered, the LES method becomes a *Very Large Eddy Simulation* since only the very large eddies (very low frequency motions) are simulated. Likewise, there are methods called, *Large Eddy Simulation with Near Wall Resolution* and *Large Eddy Simulation*

with Near Wall Modelling, each having different advantages and disadvantages.

Although some commercial codes having LES capability are present today, LES is still not widely used in the industrial world. Its usage is still confined to research works.

A more recent method is numerical simulation techniques is the *PDF Method*, where PDF stands for the probability density function. This method is developed by Stephen Pope. The idea of this method is, since the turbulent motion is a random process, instead of directly calculating the velocity field, calculating the probability density function of the velocity (and other quantities of course). The solution is not a single value for each point in the flow domain, but the range of values that a quantity might have. This method is said to be superior to Reynolds Stress models and useful especially in the modelling of dispersion and combustion problems ([8]).

1.5.3 Second Order Modelling

The attempts to solve the full Navier-Stokes equations have been explained in the previous sections. But as explained, the solutions require a heavy computational power in numerical simulations. The next method is not a direct attempt to solve the full Navier-Stokes equations but it is directed to RANS equations. As explained in section 1.2, with averaging operation, the effects of turbulence can be confined to a single term, namely the Reynolds stress term ($\langle u_i u_j \rangle$). The technique in *Second Order Modelling* (also called as *Reynolds Stress Modelling*), this term is directly modelled for each component of the Reynolds stress tensor. The modelling is based on the exact equation for the Reynolds stress tensor which

can be calculated by multiplying the linear momentum equations of Navier-Stokes equations with the appropriate momentum equation and applying the averaging operation ([30]). The resulting equations can be grouped together in the form given in (1.6).

$$\frac{D\langle\tilde{u}_i\tilde{u}_j\rangle}{Dt} = P_{ij} + \Pi_{ij} + D_{ij} + \varepsilon_{ij} + \vartheta_{ij} \tag{1.6}$$

where

$$\begin{aligned}
P_{ij} &= -\left(\langle\tilde{u}_i\tilde{u}_k\rangle\frac{\partial\langle U_j\rangle}{\partial x_k} + \langle\tilde{u}_j\tilde{u}_k\rangle\frac{\partial\langle U_i\rangle}{\partial x_k}\right) \\
\Pi_{ij} &= -\frac{1}{\rho}\left(\left\langle\tilde{u}_i\frac{\partial\tilde{p}}{\partial x_j}\right\rangle + \left\langle\tilde{u}_j\frac{\partial\tilde{p}}{\partial x_i}\right\rangle\right) \\
D_{ij} &= -\frac{\partial}{\partial x_k}\langle\tilde{u}_i\tilde{u}_j\tilde{u}_k\rangle \\
\varepsilon_{ij} &= -2\nu\left\langle\frac{\partial\tilde{u}_i}{\partial x_k}\frac{\partial\tilde{u}_j}{\partial x_k}\right\rangle \\
\vartheta_{ij} &= \nu\frac{\partial^2\langle\tilde{u}_i\tilde{u}_j\rangle}{\partial x_k^2}
\end{aligned}$$

and

P_{ij} is the production tensor. As the name implies, this term is responsible for the supply of energy to the Reynolds stresses.

Π_{ij} is the pressure-rate-of-strain tensor. It represents the effect of the fluctuating pressure on the Reynolds stresses.

D_{ij} is the turbulent diffusion tensor. It represents the diffusion in the Reynolds stresses due to turbulence.

ε_{ij} is the dissipation tensor. It represents the energy removal from the Reynolds stresses.

ϑ_{ij} is the viscous diffusion tensor. It represents the diffusion in the Reynolds stresses due to molecular diffusion.

Each term in (1.6) is treated separately,. Some of them are calculated directly (Like P_{ij}) and some of them are modelled (Like D_{ij} which is actually impossible to calculate directly and the triple correlation term is the source of the closure problem).

Reynolds stress models are superior to simpler models in complex flows such as flows with significant mean streamline curvature, flows with strong swirl or mean rotation, secondary flows in ducts and flows with rapid variations in the flow ([22]). However the numerical solution with second order models have heavier numerical constraints and it is difficult to prescribe appropriate boundary conditions, even from experimental data ([8]).

1.5.4 Turbulent Viscosity Models

The methods explained in the preceding chapters were more or less based on the exact equations of fluid motion. The modelling came into play in the details of the techniques like modelling of small scale motions in LES or the modelling of the triple velocity correlation in Reynolds Stress Modelling. *Turbulent Viscosity Models* differs from the previous methods in the way that modelling comes in the first place. Turbulent Viscosity Hypothesis, on which the turbulent viscosity models are based, approach the problem from the RANS perspective and states

that turbulent shear stress can be written similar to the laminar shear stress with the definition of a *turbulent Viscosity* :

$$\tau_{Laminar} = \mu \cdot \left(\frac{\partial \langle U_i \rangle}{\partial x_j} + \frac{\partial \langle U_j \rangle}{\partial x_i} \right)$$

$$\Rightarrow \qquad \tau_{Turbulent} = \mu_T \cdot \left(\frac{\partial \langle U_i \rangle}{\partial x_j} + \frac{\partial \langle U_j \rangle}{\partial x_i} \right) \tag{1.7}$$

With this approach, which is proposed by Boussinesq in 1877, the problem of modelling of turbulent motion reduces to modelling of a single scalar, μ_T. However this approach brings important limitations to the modelling.

The physical interpretation of the laminar (or molecular) viscosity is related to the diffusion of molecules. The unit of viscosity is m^2/s and it is composed of a length scale and a velocity scale, i.e.

$$\nu = l \cdot u \tag{1.8}$$

This composition comes from the stochastic random walk model for the diffusion of a molecule. In turbulent viscosity hypothesis, the turbulent motion is modelled as a diffusion process of eddies which are defined as the bulk of fluid that shares a common velocity for a specific time which is analogous to molecules in the molecular diffusion process.

With the definition of turbulent viscosity, Reynolds Stress Tensor can be written as,

$$\rho \langle \tilde{u}_i \tilde{u}_j \rangle = -\mu_T \cdot \left(\frac{\partial \langle U_i \rangle}{\partial x_j} + \frac{\partial \langle U_j \rangle}{\partial x_i} \right) \tag{1.9}$$

This modelling technique has various implications. First of all, it can be directly seen that it is implicitly assumed that the Reynolds Stress Tensor is

determined by the local mean rate of strain. However DNS results indicate that it is determined by the total amount of mean strain rate. Furthermore if mean rate of strain rate is changed rapidly, it takes time for turbulence to adapt itself ([8]). In addition to that five independent components of Reynolds Stress Tensor and the mean rate of strain are related to each other through a scalar variable, which is shown experimentally to be invalid even for simple shear flows ([22]).

Despite its deficiencies, Turbulent Viscosity Models is proved to be very useful especially for shear flows. For this type of flows, the only important component of the Reynolds Stress Tensor is the $\langle \tilde{u}\tilde{v} \rangle$ component.

A large portion of the research in turbulence modelling is devoted to modelling of ν_T and various modelling techniques are developed which shall be discussed in the subsequent sections.

Algebraic Models

As explained previously, the turbulent viscosity can be written as the multiplication of a length scale and a velocity scale. These length and velocity scales are remained to be determined. The theories of Prandtl (1925) and of Taylor (1935) lead to the same idea even if their phenomenology were different ([8]). For the determination of the length and velocity scales, they proposed the idea that the energy containing turbulent motions and the mean shear share the same time scale ([8]) :

$$\frac{u}{l} \approx \left| \frac{\partial \langle U \rangle}{\partial y} \right| \qquad \& \qquad \nu_T \approx u \cdot l$$

$$\Rightarrow \nu_T \sim l_m^2 \cdot \left| \frac{\partial \langle U \rangle}{\partial y} \right| \tag{1.10}$$

Hence the determination of velocity and length scale reduces to calculation of a single length scale (l_m), which is called the *mixing length*. However there is no expression is given for l_m in the original theory, therefore the equations remained to be unclosed. Furthermore an experimental constant is needed to relate the ν_T with the mean shear. But also from theoretical point of view, mixing length hypothesis indicates (From dimensional) analysis that the production and dissipation of turbulence is in local equilibrium. But it is known that kinetic energy of turbulence can be transported by the mean flow or the fluctuating motion. Therefore the models based on mixing length hypothesis are not suited for complex turbulent flows ([8]).

Although the mixing length approximation does not bring any closure in its original form, many modelling approaches are proposed which are based on the mixing length hypothesis. Although many algebraic models exists, most popular, two of them will be explained. The first model is the *Cebeci-Smith* model. In this model, the boundary layer is divided into an inner layer and an outer layer and the turbulent viscosity is written as , ([30]),

$$\nu_T = \begin{cases} \nu_{Ti} & , \quad y \leq y_m \\ \nu_{To} & , \quad y > y_m \end{cases}$$

where y_m is the smallest value of y for which $\nu_{Ti} = \nu_{To}$.

The inner layer equations are written as in the mixing length hypothesis, but using the magnitude of the mean strain :

$$\nu_{Ti} = l_m^2 \cdot \sqrt{\left(\frac{\partial \langle U \rangle}{\partial y}\right)^2 + \left(\frac{\partial \langle V \rangle}{\partial x}\right)^2} \tag{1.11}$$

Mixing length (l_m) is calculated using the Van Driest damping function as,

$$l_m = \kappa \cdot y \left[1 - e^{-y^+/A^+}\right] \tag{1.12}$$

with $\kappa = 0.4$, and $A^+ = 26$ for flows without pressure gradient.

For the outer solution, a formulation based on the Klebanoff intermittency factor and the velocity thickness is used. The model uses 3 closure coefficients.

The drawback of this approach is that the boundary layer thickness should be known a priori (For the calculation of the velocity thickness). In order to remove this drawback, Baldwin- Lomax model is proposed ([5]). In this model, again the boundary layer is divided into an inner and an outer layer. The inner layer expression is very similar to the one in the Cebeci-Smith model. However instead of the magnitude of the mean strain, the magnitude of the mean vorticity is used, i.e.

$$\nu_{Ti} = l_m^2 \cdot \sqrt{\left(\frac{\partial \langle U \rangle}{\partial y} - \frac{\partial \langle V \rangle}{\partial x}\right)^2} \tag{1.13}$$

However the real difference between the Cebeci-Smith model comes from the outer equations, where the a wake function is used in replace of the velocity thickness term. Hence the dependence on the boundary layer thickness is removed.

The Baldwin-Lomax model uses 5 closure coefficients.

Although the algebraic turbulence models have limitations, they are very useful in especially for shear flows. But it should be kept in mind that these models

are usually fine tuned for certain types of flows and the accuracy degrades for the other type of flows.

One-Equation Models

It is first proposed by Kolmogorov (1942) and Prandtl (1945) that the velocity scale in the turbulent viscosity expression should be expressed in terms of the turbulent kinetic energy :

$$u \sim \sqrt{k} \qquad \Rightarrow \qquad \nu_T = c \cdot \sqrt{k} \cdot l_m \tag{1.14}$$

The exact equation for k includes triple velocity correlations (closure problem). Therefore it can not be solved directly. But the correlation terms are present in the transport term of the k equation. In modelling, this term is replaced using the gradient-diffusion hypotheses which states that,

$$Transport \quad = \frac{\partial}{\partial x_i}\left[D_k \frac{\partial k}{\partial x_i}\right]$$

D_k can be linked to ν_T through an experimental constant. Hence the transport term can be written as :

$$Transport \quad = \frac{\partial}{\partial x_i}\left[\frac{\nu_T}{\sigma_k} \frac{\partial k}{\partial x_i}\right]$$

The other problem in the k equation is the dissipation term ε. At high Reynolds number, the dissipation rate scales with u^3/l. Since k scales with u^2, it is reasonable to write ε as ([22]),

$$\varepsilon = C_D k^{3/2}/l_m \tag{1.15}$$

With these assumptions, the one equation turbulence model can be written as,

$$\begin{aligned} \nu_T &= c \cdot \sqrt{k} \cdot l_m \\ \frac{Dk}{Dt} &= \nu_T \left(\frac{\partial \langle U_i \rangle}{\partial x_j} + \frac{\partial \langle U_j \rangle}{\partial x_i} \right) \frac{\partial \langle U_i \rangle}{\partial x_j} + \frac{\partial}{\partial x_i} \left[\frac{\nu_T}{\sigma_k} \frac{k}{x_i} \right] - C_D \frac{k^{3/2}}{l_m} \end{aligned} \tag{1.16}$$

The values of experimental constants are, $c = 1$, $\sigma_k = 1$ and $C_D = 0.07 \sim 0.09$

However the model is not complete since l_m still remains to be determined.

Another model which is also referred as *One-Equation Turbulence Model* is the model of Spallart and Allmaras proposed in 1994 (though the idea goes back to 1960s). It is based on modelling ν_T directly as,

$$\frac{D\nu_T}{Dt} = \nabla \cdot \left(\frac{\nu_T}{\sigma_\nu} \nabla \nu_T \right) + S_\nu$$

where the source term S_ν depends on the molecular and turbulent viscosity, the mean vorticity, the gradient of the turbulent viscosity and the distance from the nearest wall ([22]). It is developed specifically for aeronautical applications and it gives quite successful results in these type of applications. Unfortunately it has limitations as a general model and the results are unacceptable for other type of flows ([22]).

To distinguish the one equation model of Kolmogorov and Prandtl with Spallart and Allmaras' model, the former is usually named *Turbulent Kinetic Energy Model*.

Two-Equation Models

The two-equation turbulence models are developed after the turbulent kinetic energy model, in order to specify the length scale which is left open in turbulent

kinetic energy model. The two-equation models differ from each other in specifying the length scale. But in all models, a differential equation is written for the length scale quantity. But all the model equations have the same form :

$$\begin{aligned} \text{Total Derivative of the Length Scale Quantity} &= \text{Production} + \text{Diffusion} \\ &- \text{Dissipation} \end{aligned}$$

Although many quantities are proposed for the length scale quantity, the two of the most popular ones, $k-\varepsilon$ and $k-\omega$ will be explained.

The most widely used two-equation model is the $k-\varepsilon$ model. The basic idea of the model is that turbulence in spectral equilibrium has a one-time scale hence it can be written that ([8]), $\frac{u}{\sim}\frac{k}{\varepsilon}$

Then ν_T can be written as,

$$\nu_T \sim u \cdot l = u^2 \cdot \frac{l}{u} \qquad \Rightarrow \qquad \nu_T = C_\mu \frac{k^2}{\varepsilon} \tag{1.17}$$

The model equation for ε can be written similar to the k equation as,

$$\frac{D\varepsilon}{Dt} = C_{\varepsilon_1} C_\mu k \left(\frac{\partial \langle U_i \rangle}{\partial x_j} + \frac{\partial \langle U_j \rangle}{\partial x_i} \right) \frac{\partial \langle U_i \rangle}{\partial x_j} + \frac{\partial}{\partial x_i} \left[\frac{\nu_T}{\sigma_\varepsilon} \frac{\partial \varepsilon}{\partial x_i} \right] - C_{\varepsilon_2} \frac{\varepsilon^2}{k} \tag{1.18}$$

Five model constant have standard values of $C_\mu = 0.09$, $C_{\varepsilon_1} = 1.44$, $C_{\varepsilon_2} = 1.92$ and $\sigma_\varepsilon = 1.3$. These model constants are calculated from different flow condition where the analytical solutions exists and that the terms are isolated from each other, like homogenous isotropic turbulence of Logarithmic region of a boundary layer.

$k-\varepsilon$ model is the most extensively used two-equation model and it gives fairly accurate results for the simple flows. However for complex flows, the calculated profiles can be inaccurate even qualitatively. The inaccuracies stem from the inherent turbulent viscosity hypotheses and the equation for ε ([22]). It is also stated in [30] that $k-\varepsilon$ model is inappropriate for flows with adverse pressure gradient.

Another drawback of the $k-\varepsilon$ model is that it is not accurate at near wall regions. To compensate for this behavior, various wall-functions are proposed, which applies damping to the ε which have different accuracies ([23]). But it can be said that $k-\varepsilon$ does not give accurate results for the near-wall region of the flow but it is quiet accurate as the free stream is approached.

The other two-equation model required to be mentioned is the $k-\omega$ model. It is originally proposed by Kolmogorov that the length scale should be linked to the vorticity, ω. He also proposed a model equation for ω. But the form of the equation is changed in time and the current state of the art model is proposed by Wilcox ([30]). His model has the same form as the general form mentioned before :

$$\frac{D\omega}{Dt} = \alpha\frac{\omega}{k}\cdot\nu_T\left(\frac{\partial\langle U_i\rangle}{\partial x_j}+\frac{\partial\langle U_j\rangle}{\partial x_i}\right)\frac{\partial\langle U_i\rangle}{\partial x_j}+\frac{\partial}{\partial x_i}\left[\left(\nu+\frac{\nu_T}{\sigma_\omega}\right)\frac{\partial\omega}{\partial x_i}\right]-\beta\cdot\omega^2$$

with

$$\nu_T = \frac{k}{\omega}$$

Five model constant have standard values of $\alpha = 5/9$, $\beta = 3/40$ and $\sigma_\omega = 1/2$. These experimental constants are calculated similar to the ones in the $k-\varepsilon$ model.

The advantage of the $k-\omega$ model is that it can be integrated all through the

viscous sublayer without a need for a wall function. It gives better results than the $k-\varepsilon$ especially in adverse flow conditions ([29]).

However there are difficulties in $k-\omega$ model as the freestream and the wall is approached. As the freestream is approached, both k and ω approaches zero value which brings singularity to the turbulent viscosity since it is expressed as $\nu_T = k/\omega$. A nonphysical, non-zero value should be specified for ω to avoid this singularity. However the results depend on this value ([19]). For $k-\varepsilon$ model, no such dependence is present ([22]).

The other problem is that ω has the theoretical boundary condition of infinity at the wall. The numerical implementation of this boundary condition is through the specification of the ω value at the first grid point from the wall and the specified value depends on the distance from the wall. However in [26] it is stated that solutions are not grid independent.

The drawback of $k-\omega$ at the freestream and the $k-\varepsilon$ at near the wall led Menter to combine the two formulations ([20]). This can be achieved since ω and ε are linked each other through $\omega = \varepsilon/k$. The equation for ε can be written in terms of ω or vice versa with the use of this relation. However, for example, if ε equation is written in terms of ω, the original ω in the $k-\omega$ model is not recovered. With such formulation, an additional term emerges in the form of :

$$2 \cdot \sigma \frac{1}{\omega} \frac{\partial k}{\partial x_j} \frac{\partial \omega}{\partial x_j}$$

where σ is a model constant. This term is used with a blending function taking value between 0 and 1. For the blending function equal to 0, the original $k-\omega$ model is recovered and for 1, the model becomes the original $k-\varepsilon$ model. With

this form, the model equations starts with $k-\omega$ model from the wall and it is converted to $k-\varepsilon$ model smoothly while freestream is approached. With this approach, the advantages of both models can be acquired. This new form of the two models are called the $k-\omega$ SST (Shear Stress Transport) model.

As a final comment on two-equation turbulence models; all two-equation models share the common weakness that during an iterative solution of the variables, if any turbulent quantity becomes negative, the equations become hyperbolic and the solution diverges ([15]). A practical solution to this problem is making a change of variables to variables having non-negative values (like using the logarithm of the original variables), which changes the form of the equations.

1.5.5 The New Model

The arguments mentioned in previous sections about the turbulence models indicates a general view on the turbulence models which are summarized below :

- There are numerous turbulence models and modelling techniques having different complexity and accuracy levels.
- There is no single model that can be practically applied to any kind of flows.
- Even very simple models can achieve quite reasonable results for certain types of flows.
- Even virtually simple models can be quite complex with the addition of external modification on the flows (Like wall functions).

This character of turbulence modelling can be viewed as evidence of the idea that the research in this field should not only focus on the models having increasing complexity but also in the direction of simpler models.

With this point of view, a project on the development of a very simple model is held by Prof. Dr. Cahit Çıray from the Aerospace Engineering Department of Middle East Technical University of Turkey. The idea behind his approach is that for most of the flow types within the interest of -especially aerospace- engineering (Like boundary layer flows, jets etc.), the Reynolds Stress have a common profile, which is a profile having a single extremum point and which have zero value at the freestream and the wall (Figure 1.3).

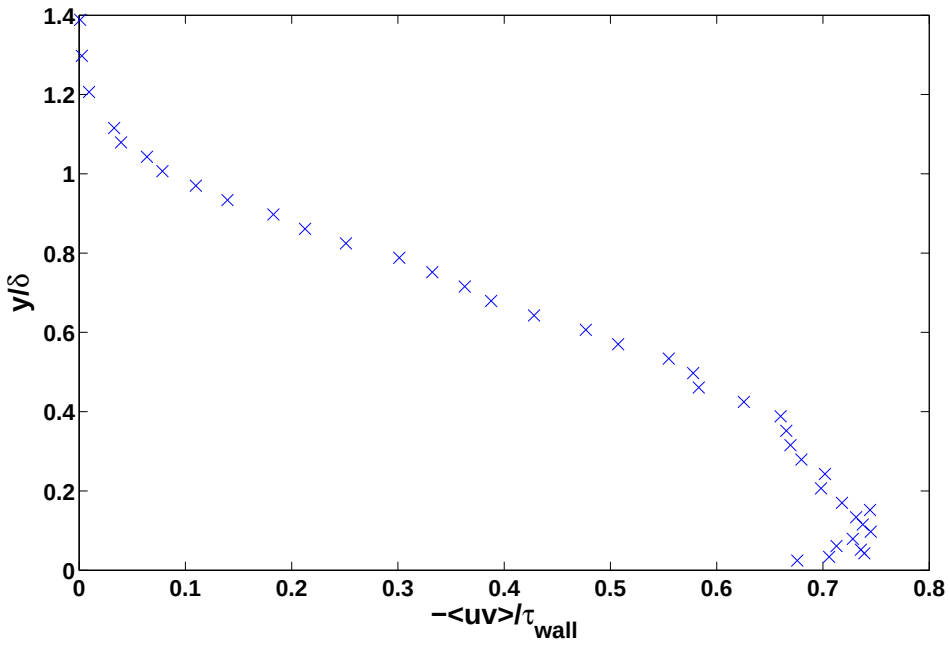

Figure 1.3: A typical Reynolds stress profile (Profile for Flat Plate flow, taken from [1])

The early attempts to find such a function is resulted in a formulation as ([3]),

$$\tau_T = -\rho\langle\tilde{u}\tilde{v}\rangle = \rho k u_\tau^2 \left[\frac{\langle U\rangle}{U_e}\left(1-\frac{y}{\delta}\right)\right] \tag{1.19}$$

In [3] the New Model was compared with experimental data for channel flows. It was shown that quite accurate results can be achieved. The next step was the application of this model to zero pressure gradient boundary layer flows. This is done in [16] and it was shown that the experimental constant k has a value of 1.4 for flat plate boundary layer flows. This thesis explains the third step in the verification of the model; application of the model to the flat plate on which pressure gradient is applied.

The details of the behavior of the model will be explained in Chapter 2.

CHAPTER 2

CHARACTERISTICS OF THE NEW MODEL

2.1 General Characteristics of the New Model

The equation for the New Turbulence Model is repeated in (2.1) for convenience [1].

$$\tau_T = -\rho\langle uv\rangle = \rho \cdot u_\tau^2 \cdot k \cdot \left[\frac{U}{U_e}\left(1-\frac{y}{\delta}\right)\right] \tag{2.1}$$

The experimental constant k is found as 1.4 for boundary layer flows without pressure gradient ([16]).

The parameters of (2.1) can be cast into two, in terms of their dependence on the spatial coordinates as,

$$\tau_T = \underbrace{\rho \cdot k}_{\text{Constant}} \cdot \underbrace{\frac{u_\tau^2}{U_e}}_{\text{x dependence}} \cdot \underbrace{U \cdot \left(1-\frac{y}{\delta}\right)}_{\text{y dependence}}$$

Note that x dependence of U_e is only present for flows with pressure gradient.

It can be seen that in the new model, the scaling is done through the external velocity (U_e) and the boundary layer thickness (δ). The major x dependence is

through u_τ.

The simple form of the turbulence model permits the comparison of the model with the theoretical works based usually on the similarity hypothesis. In such theoretical works, the boundary layer is divided into two, an *Inner Layer* and an *Outer Layer* which are shown in Figure 3.6. Then appropriate scaling laws are sought to find similarity laws in these regions.

Actually these similarity approaches are successful especially in the region, which lead to the famous *Law of the Wall*. Law of the wall is a similarity solution for the streamwise velocity but there exists certain forms for the Reynolds stresses as well. For example in [27], the Reynolds stress is given in the form of,

$$\langle uv \rangle = u_t^2 \cdot g_{12}\left(\frac{y}{\delta}\right) \tag{2.2}$$

where u_t is the velocity scale of the turbulence and g_{12} is the similarity function. Furthermore, the characteristic length and velocity scales in the inner and outer region is given in [9] as shown in Table 2.1.

Table 2.1: Characteristic length and velocity scales (taken from [9])

	Inner Layer	Outer Layer
Characteristic Velocity	u_τ	u_τ, U_e
Characteristic Length	ν/u_τ	δ

Striking similarity between (2.1) and (2.2) with Table 2.1 can be seen for outer layer solution. More recently, it has been shown that the outer layer scaling for $\langle uv \rangle$ might have a U_e^2 scaling ([13]). However it was also shown that for the

matching of the inner layer solution with the outer layer solution, the characteristic velocity should be in the form of u_τ^2. Furthermore, the scaling in length is with y/δ in [9], [27] and [13] which are all consistent with the new model. For the inner solution, the characteristic velocity is given as u_τ ([9]) and the x dependence should be on u_{tau}^2 ([13]) which is also consistent with the model. However the length scale is given as ν/u_τ which is not consistent with the model.

For boundary layers with pressure gradient, the work is confined to, so called *Equilibrium Boundary Layers*. It is defined as the flows where Cole's equilibrium parameter is constant :

$$\left(\frac{\delta}{\rho u_\tau^2}\right)\frac{dP}{dx} = constant$$

For the boundary layers with pressure gradient, there is not much source in the literature. The results of zero pressure gradient boundary layers are generalized to boundary layers with pressure gradient only in [12]. However they also have difficulty in providing a general form that recovers the zero pressure gradient case results as $\frac{dP}{dx} \to 0$. Yet there are interesting results in [12] that the Reynolds stress should have an explicit $\frac{dP}{dx}$ dependency. This dependency is not usually present in turbulence models based on turbulent viscosity hypothesis, except $k-\omega$ model where a pressure correction is proposed in [29]. However this does not mean that the solution with the New Model does not depend on pressure gradient. In fact pressure gradient affects the velocity profile and this alters the turbulence model calculations through explicit dependence on U. Most of the other turbulence models based on turbulent viscosity hypothesis have dependence on the derivative

of the mean velocity. Therefore this feedback mechanism is not that strong.

After this general view of the model, it is appropriate to look into the behavior of the model at the boundaries since unappropriate behavior of the model in these regions results in unacceptable solutions.

2.2 The Behavior of the Model at The Boundary Layer Edge

The behavior of a turbulence model as the boundary layer edge is approached, can be very problematic. In fact, the physics of this region is problematic. This region is very much affected by the intermittency, which is the unsteady behavior of the fluid that goes from laminar to turbulent state continuously. Such a behavior can not be predicted with a steady solution of the flowfield. Furthermore it is assumed in the boundary layer theory that the effects of turbulence diminishes as the edge of the boundary layer is approached. However experimental results does not indicate such behavior as shown in Figure 2.1. Experimental data indicates that turbulent shear stress have a finite value and finite nonzero derivative at the boundary layer edge. This can also seen from the boundary layer equations.

At boundary layer edge, the derivative of the mean streamwise velocity is zero and the mean stream wise velocity is equal to the edge velocity :

$$-U\frac{\partial V}{\partial y} + \underbrace{\frac{\partial U}{\partial y}}_{\to 0} V = \underbrace{\nu\frac{\partial^2 U}{\partial y^2}}_{\to 0} - \frac{1}{\rho}\frac{dP}{dx} + \frac{1}{\rho}\frac{\partial \tau_T}{\partial y}$$

$$\Rightarrow -U_e\frac{\partial V}{\partial y} + \frac{1}{\rho}\frac{dP}{dx} = \frac{1}{\rho}\frac{\partial \tau_T}{\partial y}$$

However $\frac{\partial V}{\partial y}\Big|_{y=\delta} \neq 0$, which will be discussed in section 3.1.2. Since $U_e \frac{\partial V}{\partial y} \neq \frac{1}{\rho}\frac{dP}{dx}$ in general, then, $\frac{\partial \tau_T}{\partial y} \neq 0$ in general. However it is difficult to find a suitable boundary condition for the derivative of the transverse velocity, hence for the derivative of the turbulent shear stress therefore it is best to apply zero derivative condition for the turbulent shear stress at the boundary layer edge.

The derivative of the τ_T from the model equation can be directly calculated as,

$$\frac{\partial \tau_T}{\partial y} = \frac{\rho u_\tau^2 k}{U_e}\left[\frac{\partial U}{\partial y}\left(1-\frac{y}{\delta}\right) - \frac{U}{\delta}\right]$$

$$\text{For} \quad y \to \delta \qquad \Rightarrow \frac{\partial \tau_T}{\partial y} = -\frac{\rho u_\tau^2 k}{\delta} \neq 0$$

To damp the predictions of turbulence models near the boundary edge, a correction is usually applied, which is called *Klebanoff Intermittency Function* ([30]). This correction is in the form of a factor as,

$$F_{Klebanoff} = \left[1 + 5.5\left(\frac{y}{\delta}\right)^6\right]^{-1}$$

with which the predicted turbulent shear stress is multiplied. However it was seen that the Klebanoff correction increases the error between the experimental data and the model predictions, which can be seen from Figure 2.1. To avoid this, instead of Klebanoff correction, cubic spline fitting is applied to the model at from approximately $y/\delta = 0.8$ to $y/\delta = 1$ to get a smooth transition to $\tau_T = 0$ and $\frac{\partial \tau_T}{\partial y} = 0$ at $y = \delta$. [2] The comparison of the models predictions without

[2] Spline fitting is extensively used within this thesis work for the achievement of the solution of the boundary layers. Therefore the general formulation for the spline fitting is explained in Appendix A.

correction, with Klebanoff correction and with spline fitting, with experimental data is given in Figure 2.1.

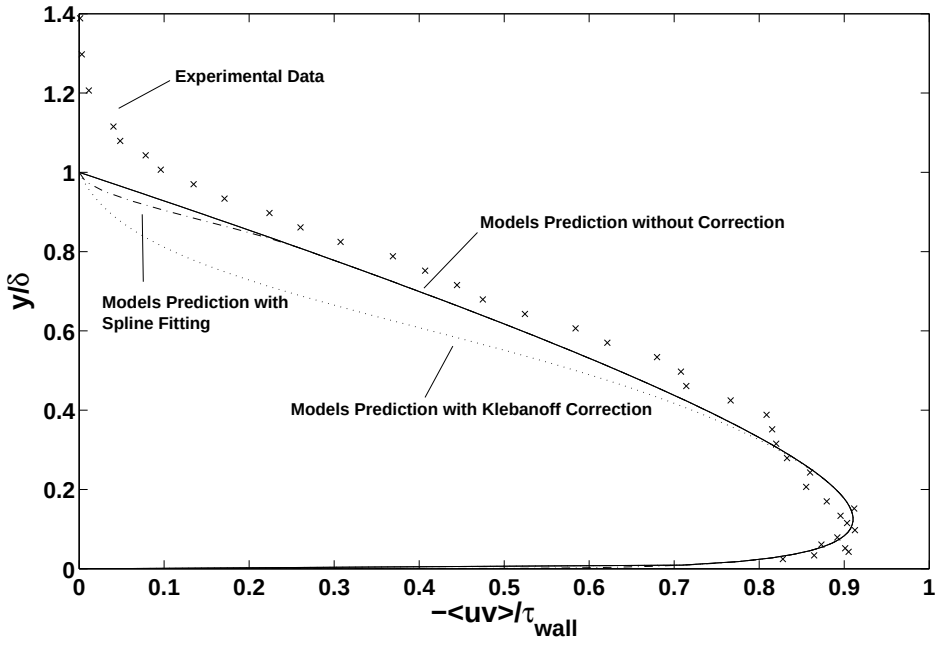

Figure 2.1: The Comparison of the New Model's turbulent shear stress predictions with experimental data taken from [1]

2.3 The Behavior of The Model Near The Wall

The near wall behavior of a model is a very key point in the characterization of the model. Because it gives a strict limitations for the grids to be used in the solution and of course the accuracy of the calculations. A large portion of the work on turbulence models are devoted the finding appropriate functions to apply damping to the model predictions, if a model does not have an appropriate asymptotic behavior as the wall is approached. Before investigating the behavior of the model as the wall is approached, it is convenient to look at the behavior of the Reynolds shear stress near the wall.

The first layer within the boundary layer from the wall is the viscous sublayer. Together with the logarithmic layer, they form the *Constant Shear Layer*. As the name implies, the shear stress in this region is constant. Actually this idea is used in the derivation of law of the wall. For the generation of the law of the wall, it is usually written that,

$$\frac{\partial \tau}{\partial y} = 0 \qquad \Leftrightarrow \qquad \tau = constant$$

However, this is only true for boundary layers without pressure gradient. For the pressure gradient case, it should be modified as ([28]),

$$\frac{\tau}{\tau_{wall}} = 1 + \xi\eta$$

where

$$\eta = \frac{y}{\delta} \qquad \& \qquad \xi = \frac{\delta}{\tau_{wall}} \frac{dP}{dx}$$

However this is merely a first order approximation and a higher order version (Third order polynomial with respect to η) to cover the whole boundary layer is also present ([28]). Another higher order approximation (It is intended to mean that the equation is valid further away from the wall with the term "higher order") can also be acquired using the logarithmic form for the velocity as ([27]),

$$\tau = \tau_{wall} + \frac{dP}{dx} + \frac{1}{\kappa} \frac{d\tau_{wall}}{dx} \left(\log y^+ + A - 1 \right) \cdot y$$

But all the formulations lack the experimental validation and it is stated in [9] that the region is so close the wall that it is not possible to take accurate measurements to verify the hypotheses. [9] dates back to 1978 and it is highly probable

that the measurement techniques are improved since then and there might be experimental verifications about the approaches however in the literature. But within the context of this thesis, they have not been investigated.

The behavior of the New Model in the near wall region can be investigated through the derivative of it :

$$\frac{\partial \tau_T}{\partial y} = \frac{\rho u_\tau^2 k}{U_e}\left[\frac{\partial U}{\partial y}\left(1-\frac{y}{\delta}\right)-\frac{U}{\delta}\right]$$

$$\text{For} \quad y \to 0 \qquad U \to 0$$

$$\Rightarrow \frac{\partial \tau_T}{\partial y} = \frac{\rho u_\tau^4 k}{U_e \nu} \neq 0$$

To suppress this asymptotically wrong behavior, wall functions can be used. However, as mentioned previously, the investigation of appropriate wall function for the turbulence models is a whole another research field and it can be a topic of a separate thesis. Since the intend of this thesis is to investigate the validity of the turbulence model, not the optimization of it for a practical problem, the simplest approach is taken. The common idea about the behavior of the shear stress is that for regions very very close to wall, the shear stress can be written to first order as $\tau = \tau_{wall} + dP/dxy$. Therefore the prediction of the model is fitted with a cubic polynomial within the region approximately $y^+ = 5$ and $y^+ = 20$. The boundary conditions for the turbulent shear stress for the spline fitting is chosen to be :

$$\tau_T|_{y\sim 5} = 0 \qquad \& \qquad \left.\frac{\partial \tau_T}{\partial y}\right|_{y\sim 5} = \frac{dP}{dx}$$

Of course such an approach is not sufficient to give a direct result. Therefore a correction is made on the calculated velocity profiles near the wall which shall be explained in section 3.1.4.

CHAPTER 3

NUMERICAL IMPLEMENTATION

3.1 Solution Technique

Governing equations of incompressible boundary layer flows are composed of a linear first order differential equation (Equation for conservation of mass or continuity equation) and a second order nonlinear differential equation (Equation for conservation of linear momentum).

$$\begin{aligned} \frac{\partial U}{\partial x} + \frac{\partial V}{\partial y} &= 0 \\ U \cdot \frac{\partial U}{\partial x} + V \cdot \frac{\partial U}{\partial y} &= -\frac{1}{\rho} \cdot \frac{dP}{dx} + \frac{\partial \tau}{\partial y} \end{aligned} \tag{3.1}$$

The second order character of (3.1) comes from the $\frac{\partial \tau}{\partial y}$ term since $\tau = \mu \frac{\partial U}{\partial y} + \tau_T$ and hence $\frac{\partial \tau}{\partial y} = \mu \frac{\partial^2 U}{\partial y^2} + \frac{\partial \tau_T}{\partial y}$ makes the equation, second order. The structure of the model equation for τ_T might also affect the order of the boundary layer equations. However the usual turbulent viscosity assumption equates this term to $\tau_T = \mu_T \frac{\partial U}{\partial y}$ hence the highest derivative is still second order. In the model that will be used

in this work, τ_T is calculated in the form of $\tau_T = f(U)$ hence the $\frac{\partial \tau_T}{\partial y}$ term brings a first order differential for U and therefore the second order character do not alter.

A second order partial differential equations can be classified according to the coefficients of the second order differential terms ([14]). A general second order quasi-linear differential equation (A differential equation is classified as *Quasi-linear* if its highest order derivative terms are linear) for the dependent variable ϕ is given in (3.2) to illustrate the case.

$$A \cdot \frac{\partial^2 \phi}{\partial x^2} + B \cdot \frac{\partial^2 \phi}{\partial x \partial y} + C \cdot \frac{\partial^2 \phi}{\partial y^2} + D \cdot \frac{\partial \phi}{\partial x} + E \cdot \frac{\partial \phi}{\partial y} + F \cdot \phi + G = 0 \qquad (3.2)$$

Coefficients A, B and C characterizes the equation and the equation is classified as follows :

$$B^2 - 4AC < 0 \quad : \quad \text{Elliptic Partial Differential Equation}$$

$$B^2 - 4AC = 0 \quad : \quad \text{Parabolic Partial Differential Equations}$$

$$B^2 - 4AC > 0 \quad : \quad \text{Hyperbolic Partial Differential Equations}$$

Boundary layer equations are parabolic in nature. Since they are composed of a first order and a second order differential equation, its parabolic character can be shown more clearly with a set of new variables, which can be found in [14].

Different solution procedures exist for different classes of differential equations. Parabolic differential equations can be numerically integrated to yield the

solution, by prescribing the initial condition and the boundary conditions that binds the solution in the domain (Figure 3.1).

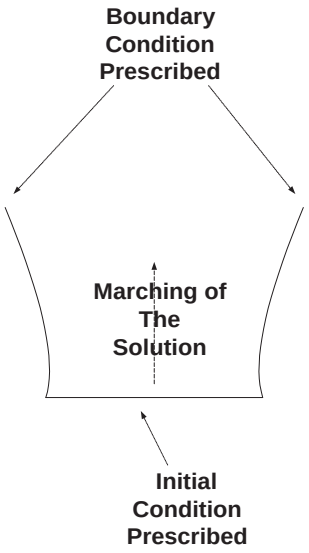

Figure 3.1: Solution domain of a parabolic partial differential equation)

Boundary layer equations can be solved similarly (Figure 3.2).

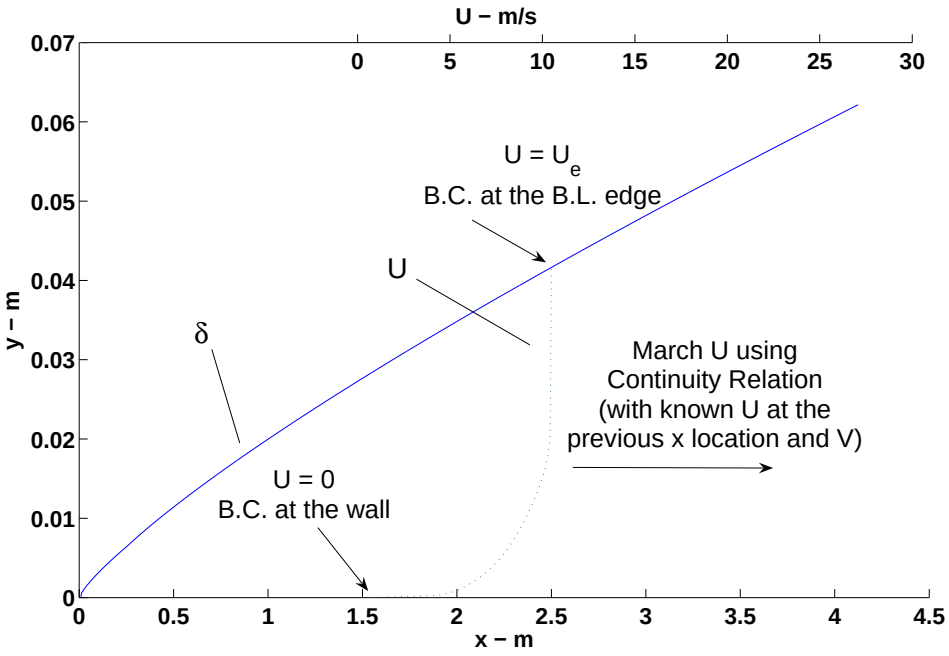

Figure 3.2: Solution of boundary layer equations

For the boundary layer equations to be solved in this manner, (3.1) can be

modified by taken the $\frac{\partial U}{\partial x}$ term from the continuity equation and plugging into the linear momentum equation.

$$\begin{aligned} \frac{\partial U}{\partial x} + \frac{\partial V}{\partial y} &= 0 \\ -U \cdot \frac{\partial V}{\partial y} + V \cdot \frac{\partial U}{\partial y} &= -\frac{1}{\rho} \cdot \frac{dP}{dx} + \frac{\partial \tau}{\partial y} \end{aligned} \tag{3.3}$$

The result is a first order partial differential equation linear in V (The coefficients of the V terms are free from any V or $\frac{\partial V}{\partial y}$ dependence) and consists of derivatives with respect to only y, except the $\frac{dP}{dx}$ term which is supplied to the equations externally. (3.3) can be solved in the following way :

1. Assign a profile for U at the beginning of the boundary layer.
2. Calculate the coefficients of V and $\frac{\partial V}{\partial y}$ in (3.3) and the right hand side of the (3.3) using the U profile for the previous x location.
3. Solve (3.3) for V.
4. Integrated the $\frac{\partial U}{\partial x}$ to the current x location, using the continuity relation.

Since the boundary layer equations can be solved with this method, as ordinary differential equations, the specific issues related the numerical solution procedure boils down to; initialization of the streamwise velocity profile ($U(y)|_{x=x_0}$), specifying the boundary conditions for the wall normal velocity ($V(y=0)|_{x=x_j}$) and $V(y=\delta)|_{x=x_j}$, integration of wall normal velocity in y direction and integration of streamwise velocity in x direction, which are explained in the following sections.

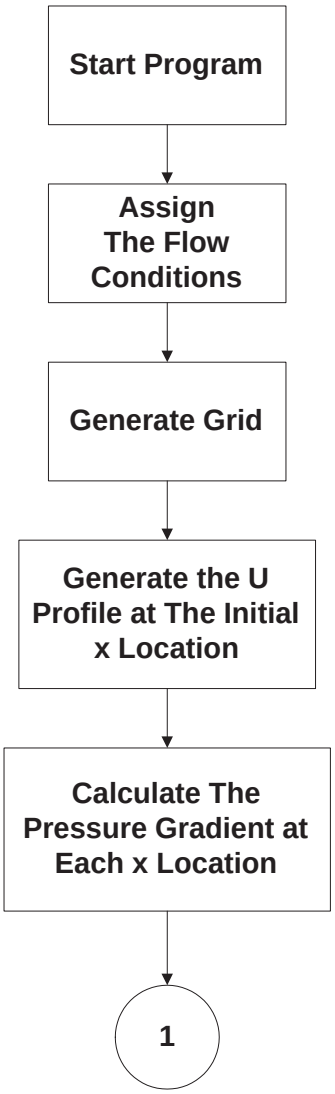

Figure 3.3: Flowchart of the Solution Procedure

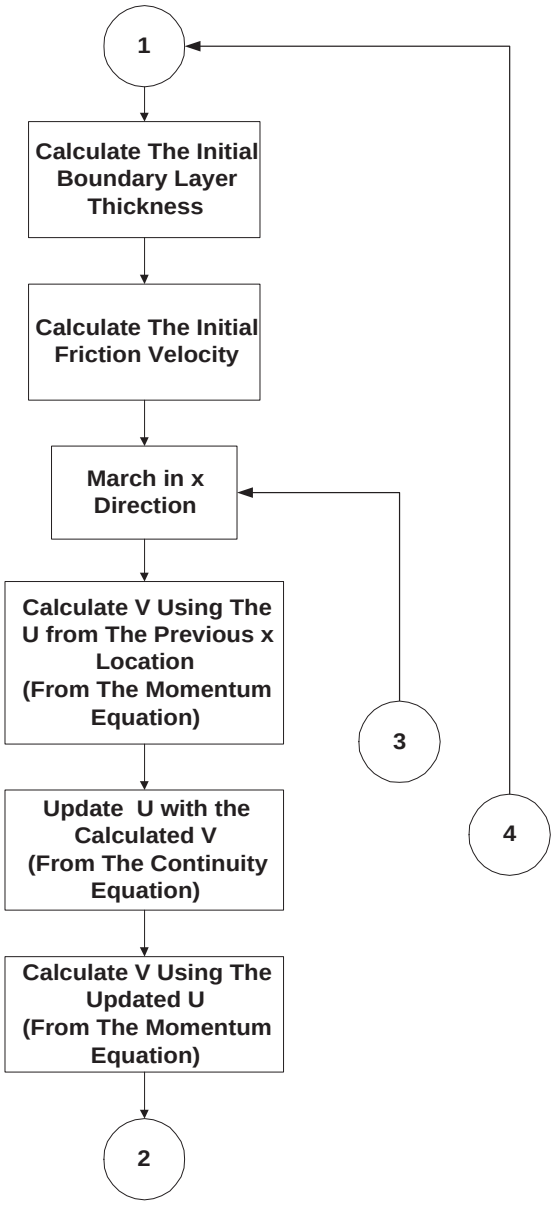

Figure 3.4: Flowchart of the Solution Procedure (Continue)

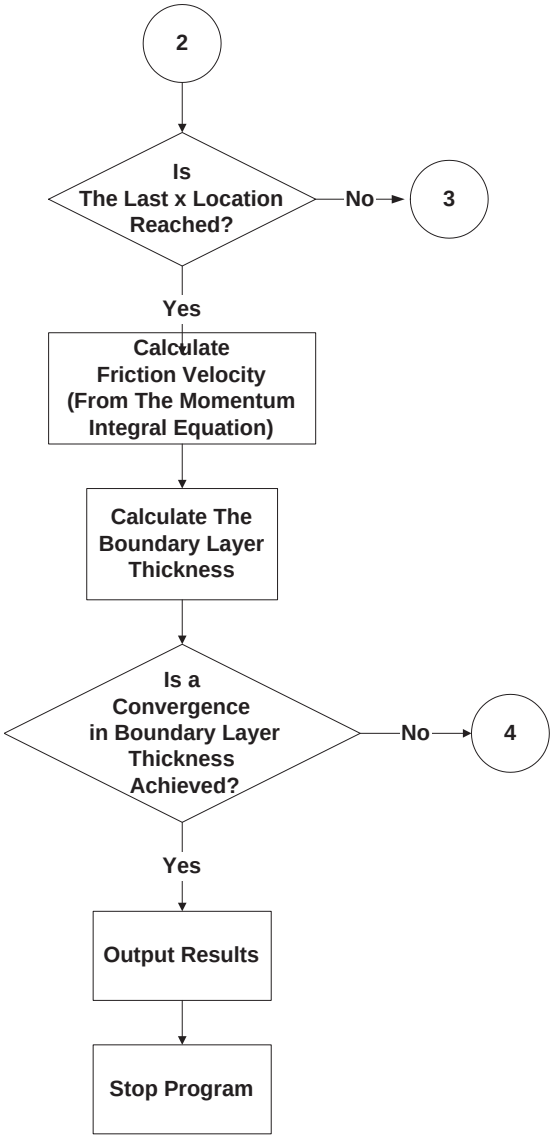

Figure 3.5: Flowchart of the Solution Procedure (Continue)

The general flowchart of the program is given in Figures 3.3, 3.4 and 3.5

The explanation of the processes shown in Figures 3.3, 3.4 and 3.5 is given below :

Assign The Flow Conditions In this part of the program; parameters that define the flow conditions, like the freestream velocity, density, viscosity and the general geometry , like the length of the flat plate, the maximum distance from the wall, are given specified.

Generate Grid The grid is generated using the geometry related parameters, like the length of the flatplate, the maximum distance from the wall, the number of grid points etc. with the method explained in section 3.2

Generate the U Profile at The Initial x Location The streamwise velocity profile at the initial x location is generated with the method explained in 3.1.1

Calculate The Pressure Gradient at Each x Location Pressure at each x location is supplied to the program externally. The pressure gradient is calculated numerically from the supplied pressure. The exact process depends on the experimental conditions simulated, which are explained in Chapter 4 for each case.

Calculate The Initial Boundary Layer Thickness The boundary layer thickness at each x location is calculated using the flat plate correlation of delta.

Calculate The Initial Friction Velocity The friction velocity at each x location is calculated using the flat plate correlation of delta.

March in x Direction The solution point moves to the next grid points in x direction

Calculate V Using The U from The Previous Location The momentum equation of the boundary layer equations is integrated for the transverse velocity (V). The streamwise velocity (U) dependent terms are evaluated with the known streamwise velocity values from the previous x location. This procedure is explained in section 3.1.2.

Update U with the Calculated V The calculated transverse velocity is used in continuity equation in order to calculate the derivative of the streamwise velocity with respect to x. This derivative is integrated to update the streamwise velocity. This procedure is explained in section 3.1.3.

Calculate V Using The Updated U The momentum equation of the boundary layer equations is integrated for the transverse velocity (V). The streamwise velocity (U) dependent terms are evaluated with the calculated values from the previous update process. This procedure is explained in section 3.1.2.

Calculate Friction Velocity After calculation of streamwise velocity field over the solution domain, all the integral parameters of the boundary layer can be calculated. These integral parameters are used in the Momentum Integral Equation to calculate the shear stress at the wall, hence the friction velocity. This procedure is explained in section 3.1.4.

Calculate The Boundary Layer Thickness The boundary layer thickness is

re-calculated with the known streamwise velocity field, from the original definition of the boundary layer thickness.

Output Results The output of the results are displayed in graphical format

3.1.1 Initial Condition for Streamwise Velocity

[1]The generation of initial profile for a specified location on the flat plate has a vital importance since the accuracy of the results on the solution domain is directly affected by the initial conditions. Although many correlations for the velocity profiles exist, they are not sufficient for the generation of a velocity profile at a specified x location on a flat plate under arbitrary flow conditions. Therefore it is required to assume two conditions in order to generate a proper velocity profile. These conditions are explained below :

The initial x location is very close to the leading edge The requirement for the initial x location to be very close to the wall comes from the dependence of the velocity profile to the pressure gradient. Although there exists correlations for the integral parameters of the boundary layer under pressure gradient ([28]), they have no use in the generation of the velocity profile. But if the initial x location is close to the leading edge, then the effect of pressure gradient on the profile can be assumed to be negligible and the formulas for the zero pressure gradient boundary layers can be used.

For solution of boundary layers with zero pressure gradient, this assumption

[1] *Initial Condition* term is usually used for the generated initial conditions for iterative solutions to start the iteration process. However in the step marching methods that will be used, it is the conditions at which the solution starts. It does not change through the solution process and therefore it can be seen as a boundary condition.

is not required.

Boundary layer is turbulent from leading edge Actually, this assumption does not come from the difficulty in the generation of the velocity profile. In fact, laminar boundary layers have similarity solutions which permits the generation of the velocity profile at an arbitrary x location under arbitrary flow conditions ([24]). However the performance of the turbulence model for the prediction of the transition from laminar to turbulent flow is not warranted and therefore it is best to study the flow to be turbulent from the beginning. This assumption will not affect the comparisons between the calculated and experimental results since in the turbulence experiments, the flow is usually made turbulent at the leading edge using a turbulator.

With these two conditions, many correlations that have been generated during the past century becomes available. But care should be taken for the validity and the behavior of these models. What required from the initial profile is not only representing the U correctly but also, $\frac{\partial U}{\partial y}$ should be represented correctly since it is used in the calculation of boundary layer equations, directly.

Before the general overview of the functions for velocity profiles for the zero pressure boundary layers, it is appropriate to look into the structure of the boundary layer.

The research during the past century resulted in a common understanding of the boundary layers with the separation of the boundary layer into sublayers where different effects dominate the structure. These layers are shown in Figure 3.6.

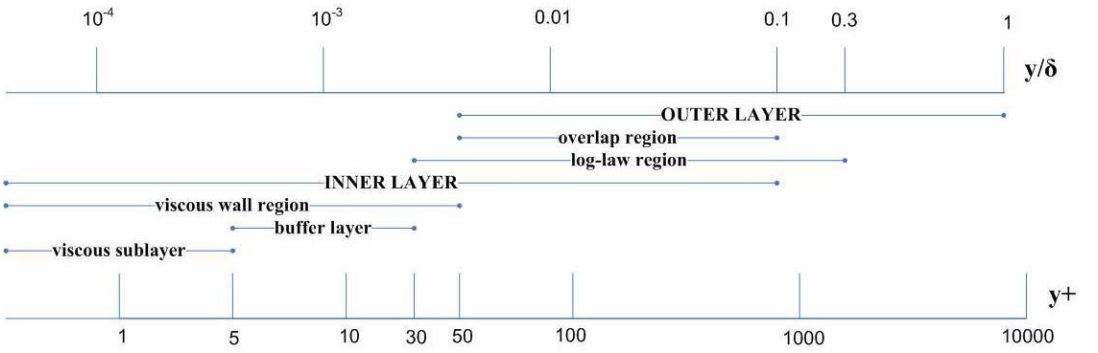

Figure 3.6: The sub-layers of a turbulent boundary layer ([22])

There are two nondimensional lengths that are used to characterize the boundary layers : Distance from the wall relative to boundary layer thickness ($\frac{y}{\delta}$) and the distance from the wall measured in viscous lengths ($y^+ = \frac{y \cdot u_\tau}{\nu}$). Actually these two length scales are appropriate units for outer and inner layers of turbulent boundary layers, respectively. Therefore the velocity profiles are formulated with respect to these variables.

The first layer from the wall is called the *viscous sublayer*. The layer starts from the wall and ends at $y^+ \approx 5$. Viscous effects dominate the flow in this region and the velocity profile can be written (in wall coordinates) as,

$$u^+ = y^+ \tag{3.4}$$

where

$$u^+ = \frac{U}{u_\tau} \qquad y^+ = \frac{y \cdot u_\tau}{\nu} \qquad u_\tau = \sqrt{\frac{\tau_w}{\rho}} = \sqrt{\nu \cdot \left.\frac{dU}{dy}\right|_{y=0}}$$

These relations result in a linear profile for $U(y)$ with respect to y.

The second layer from the wall is called the *buffer layer*. In this layer, both viscous and turbulent stresses affect the flow at the same order and it represents the transition region between the viscous sublayer and the log-law layer.

The third layer is the *log-law layer*. The viscous effects are negligible in this region and the flow is affected entirely by turbulent stresses. The velocity profile can be written as,

$$u^+ = \frac{1}{\kappa} \ln y^+ + B \tag{3.5}$$

There are variations in the literature about the values of κ and B. But they are generally within 5% of $\kappa = 0.41$ and $B = 5.2$ ([22]).

Although (3.5) is the accepted profile for the log-law region (in fact, due to (3.5), the name of the layer comes) by the scientific community, there is also an argument going on about the velocity profile for this region ([10]). In [13], it is argued that the profile should have a power-law form rather than a logarithmic form. It is not the accuracy of the formulations that make the difference between these two ideas. In fact, more than half a century of experimental work had validated the accuracy of the log-law. But the problem is, (3.5) is independent of Re and it is claimed to be universal. However a power-law relation inherently brings a Re dependence on the profile and the universality of the logarithmic region vanishes. But since this debate is not related to accuracy of the formulations, there is no reason to abandon the proven log-law relation, for the purpose of this thesis.

The rest of the boundary layer is composed of the outer layer which is affected by the boundary layer edge conditions.

For engineering applications, it is well known that a power law relation for the entire boundary layer generates suitable profiles. The relation can be written

as ([24]) :

$$U = U_\infty \cdot \left(\frac{y}{\delta}\right)^{1/n} \tag{3.6}$$

where n can be taken from various values ranging from 2 to 10, depending on the Reynolds number and the boundary layer under investigation. For zero pressure gradient flat plate solutions at moderate Reynolds numbers, values from 5 to 7 can be used 7 is taken in the calculations.

The problem with (3.6) is that although it is a good approximation for the mean velocity, it does not represent the derivative of mean velocity with respect to distance from the wall (Comparison of the power law with (3.4) is shown in Figure 3.7).

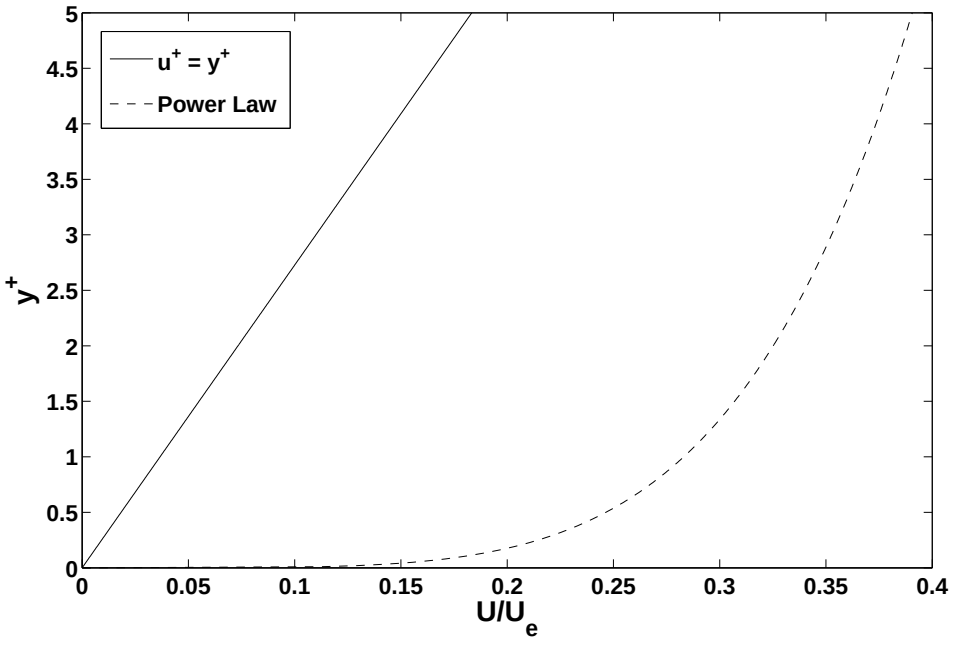

Figure 3.7: Comparison of Power Law with Law of The Wall

Table 3.1: The formulations used for the generation of initial U profile

$0 < y^+ < 5$	$u^+ = y^+$
$5 < y^+ < 30$	Spline Fitting
$30 < y^+, y/\delta < 0.08$	$u^+ = \frac{1}{\kappa} \ln y^+ + B$
$0.08 < y/\delta < 0.3$	Spline Fitting
$0.3 < y/\delta < 1$	$U = U_\infty \cdot \left(\frac{y}{\delta}\right)^{1/n}$

Three relations ((3.4), (3.5) and (3.6)) are given for different regions of the boundary layer. The best thing to do is to combine them to generate a single velocity profile. Since there are layers between the layers that the profiles are valid, the transition between the formulations should be smooth. The requirement for smooth transition is satisfied by the usage of third order spline fittings ([18]) at transition regions.

The formulations used with respect to the distances from the wall is summarized in Table 3.1.

The initial x location for the calculations to start is usually taken as $x_0 = 0.01m$.

As a final note, (3.4), (3.5) gives the false impression that u_τ is an independent parameter. Actually it is the opposite, u_τ is determined by the velocity profile. Therefore it should be explicitly supplied to the calculations. The calculation of u_τ is explained in section 3.1.4.

3.1.2 Integration of Wall Normal Velocity

With known U, the second equation of (3.3) becomes an ordinary differential equation of V in y,

$$-U \cdot \frac{dV}{dy} + \frac{\partial U}{\partial y} \cdot V = -\frac{1}{\rho} \cdot \frac{dP}{dx} + \frac{\partial \tau}{\partial y} \tag{3.7}$$

But a differential equation can not be solved without specifying the appropriate boundary conditions. The boundary conditions for the boundary layer equations are usually given as :

$$U|_{y=0} = 0 \qquad \lim_{y\to\infty} U = U_e \quad or \quad \lim_{y\to\infty} \frac{\partial U}{\partial y} = 0$$

$$V|_{y=0} = 0$$

Usually, boundary condition for V at $y = \infty$ is not defined. Intuitionally, it seems reasonable to assume

$$\lim_{y\to\infty} V = V_e \quad or \quad \lim_{y\to\infty} \frac{\partial V}{\partial y} = 0$$

and in fact in [30], the boundary condition is given in this form. However this condition is not easy to implement into a numerical solution procedure for which a finite value of boundary layer thickness is required. This will proven below, with reductio ad absurdum method.

In computations, with definition of boundary layer thickness δ, the boundary condition at boundary layer edge is written as,

$$\lim_{y\to\infty} U = U_e \equiv \lim_{y\to\delta} U = U_e \quad or \quad \lim_{y\to\infty} \frac{\partial U}{\partial y} = 0 \equiv \lim_{y\to\delta} \frac{\partial U}{\partial y} = 0$$

To use the boundary condition of V in a similar manner,

$$\lim_{y\to\infty} V = V_e \equiv \lim_{y\to\delta} V = V_e \quad \text{or} \quad \lim_{y\to\infty} \frac{\partial V}{\partial y} = 0 \equiv \lim_{y\to\delta} \frac{\partial V}{\partial y} = 0$$

should also be valid. But if this result is used in continuity relation, it can be directly found that :

$$\frac{\partial U}{\partial x} + \frac{\partial V}{\partial y} = 0 \Rightarrow \frac{\partial U}{\partial x} = -\frac{\partial V}{\partial y}$$

$$\left.\frac{\partial U}{\partial x}\right|_{y=\delta} = -\left.\frac{\partial V}{\partial y}\right|_{y=\delta} = 0$$

But for a growing boundary layer, it is not possible to $\left.\frac{\partial U}{\partial x}\right|_{y=\delta} = 0$ condition. This is shown in Figure 3.8 geometrically.

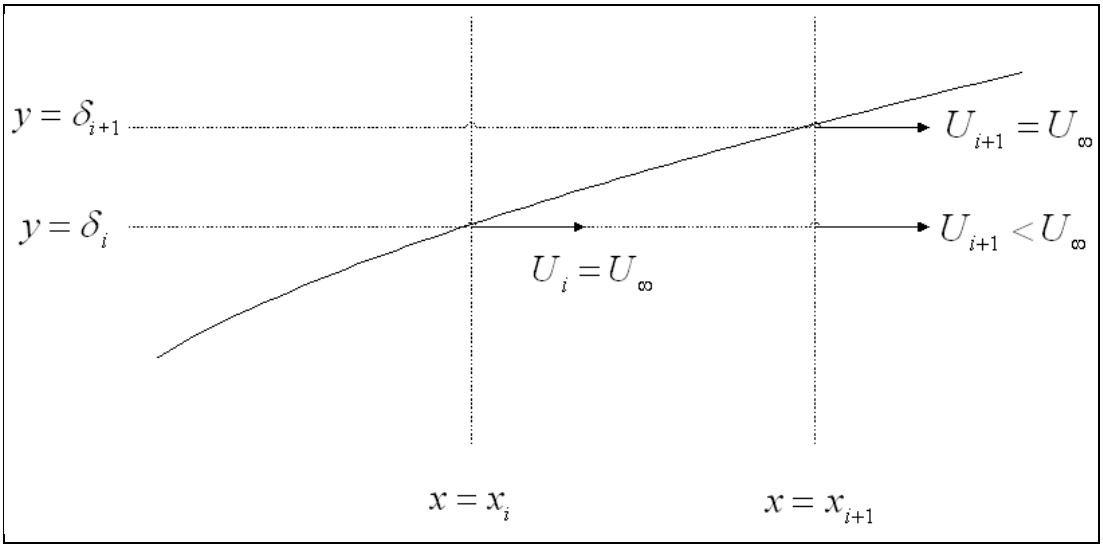

Figure 3.8: Velocity profile at the edge of a growing boundary layer

Therefore,

$$\lim_{y\to\delta} V \neq V_e \qquad \text{and} \qquad \lim_{y\to\delta} \frac{\partial V}{\partial y} \neq 0$$

This result is very unfortunate because the boundary condition of V at the boundary layer has a vital effect on the solution. To see this effect, the conditions at the other end of the boundary layer, i.e. velocity profile near the wall, should be scrutinized.

The starting point of investigation for the velocity profile of V near the wall is the behavior of U near the wall, i.e. (3.4) :

$$u^+ = y^+ \Rightarrow U = y \cdot \frac{u_\tau^2}{\nu} \Rightarrow \frac{\partial U}{\partial y} = \frac{u_\tau^2}{\nu} \quad \text{and} \quad \frac{\partial^2 U}{\partial y^2} = 0$$

Plugging the relations to (3.3) results in,

$$-y \cdot \frac{u_\tau^2}{\nu} \cdot \frac{\partial V}{\partial y} + \frac{u_\tau^2}{\nu} \cdot V = -\frac{1}{\rho} \cdot \frac{dP}{dx} + \frac{1}{\rho} \cdot \frac{\partial \tau}{\partial y} \tag{3.8}$$

Right hand side of the (3.8) is zero since,

$$\text{as} \qquad y \to 0 \qquad \frac{\partial \tau}{\partial y} = \frac{dP}{dx}$$

the proof of which can be found in [27].

With a zero right hand side, (3.8) becomes a homogenous ordinary differential equation and the common term $\frac{u_\tau^2}{\nu}$ can be eliminated. The result is given in (3.9).

$$\frac{\partial V}{\partial y} - \frac{1}{y} \cdot V = 0 \tag{3.9}$$

(3.9) can easily be integrated using the integrator function of $\ln y$. Hence the velocity profile for V approaching the wall is given by,

$$\text{as} \qquad y \to 0 \qquad V(y) = a \cdot y$$

where a is a dummy constant which should be found from the boundary conditions.

However this linear relationship satisfies the $V|_{y=0} = 0$ condition, for any finite value of a. Therefore only mechanism for the determination of the slope of V at the wall is through the boundary condition at the boundary layer edge. Unfortunately, the solution with $\lim_{y \to \delta} \frac{\partial V}{\partial y} = 0$ boundary condition gives unreasonable results. The V velocity is reversed at wall ($a < 0$) and this reversal shifts the entire solution. An example for the solution is given in Figure 3.9.

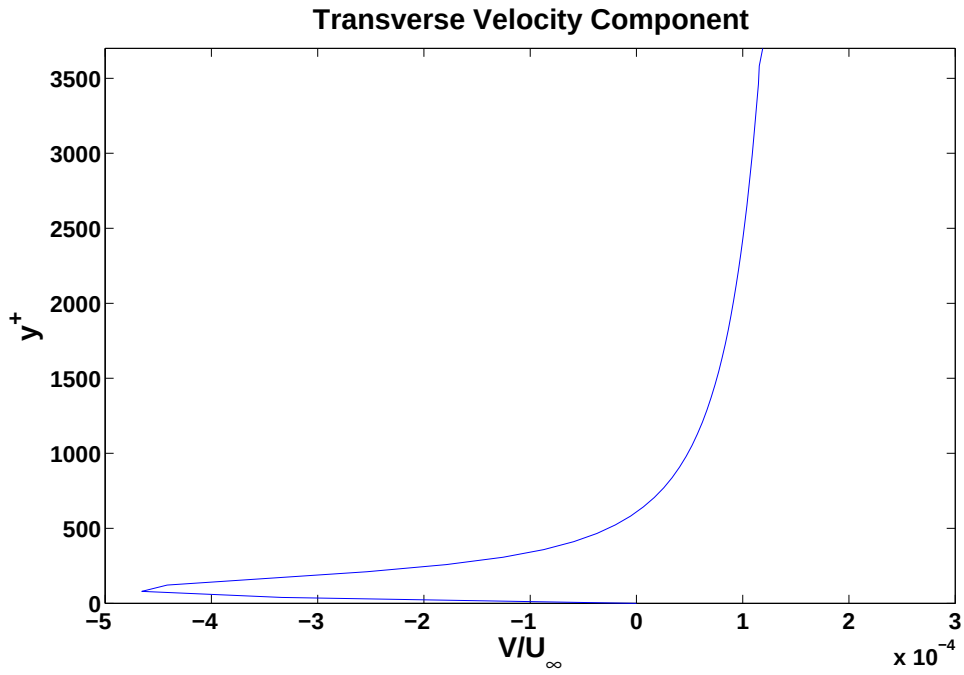

Figure 3.9: Solution of V with $\lim_{y\to\delta} \frac{\partial V}{\partial y} = 0$ boundary condition gives unacceptable results.

With this result, many solution algorithms that could be used for V, are eliminated and the only method remains is to directly integrate the equations from the wall using the wall boundary condition of V, $V|_{y=0} = 0$. The derivative of V can be written from (3.7) as,

$$\frac{\partial V}{\partial y} = \frac{1}{U} \cdot \left(V \cdot \frac{\partial U}{\partial y} + \frac{1}{\rho} \cdot \frac{dP}{dx} - \frac{\partial \tau}{\partial y} \right) \tag{3.10}$$

Many solution techniques exist for the numerical solution of a first order (like (3.10)) differential equation ([17]). They vary from simple Euler integration algorithm to more sophisticated Runge-Kutta methods. However increasing the order of the integration algorithm results in excessive recalculation of right hand side terms of (3.10). Since the V profile is a rather smooth function, low order algorithms will be sufficient. Therefore *Improved Euler* or *Heun's* method is used in the numerical solution of (3.7), which is second order accurate ([17]). Heun's

method can be summarized as follows :

Let $\frac{dy}{dx} = f(x, y)$. For the numerical solution of such a problem at a node point $n + 1$, with $dx = h$, first a dummy calculations is made,

$$y'_{n+1} = y_n + h \cdot f(x_n, y_n)$$

Then this solution is used in the update of the derivative,

$$y_{n+1} = y_n + \frac{1}{2} \cdot h \cdot [f(x_n, y_n) + f(x_n, y'_n)]$$

3.1.3 Integration of Streamwise Velocity

Once the V profile is generated for any x location, U can be integrated from the previous x location to the current one using the continuity equation :

$$\frac{\partial U}{\partial x} + \frac{\partial V}{\partial y} = 0 \qquad \Rightarrow \qquad \frac{\partial U}{\partial x} = -\frac{\partial V}{\partial y} \tag{3.11}$$

As in the integration of V, Heun's method will be used in the numerical solution of (3.11), which is explained in section 3.1.2.

3.1.4 Turbulence Model Related Issues

Apart from the general solution scheme, there are also specific issues related the turbulence model that is used. The equation for the turbulence model is given in (3.12) for convenience.

$$\tau_T = -\langle uv \rangle = \rho \cdot u_\tau^2 \cdot k \cdot \left[\frac{U}{U_e} \left(1 - \frac{y}{\delta} \right) \right] \tag{3.12}$$

As can be seen directly from the model equation, the shear velocity (u_τ) and the boundary layer thickness (δ) should be supplied to the model a priori. However these parameters are the result of the solution and they are unknowns prior to the full solution. In addition this problem, as mentioned in section 2.3,

the model equation has a problem at the near wall region. This problematic behavior should be corrected in order to achieve appropriate results. These issues will be discussed in the subsequent sections.

Calculation of the Boundary Layer Thickness

The estimation of the boundary layer thickness is a very important problem in the boundary layer calculations since it indicates the region of validity for many turbulence quantities. It has an extra importance for the New Model since the formulation of the model has an explicit dependence on the boundary layer thickness.

For flat plates with zero pressure gradient, the problem of determination of δ can be solved using correlations such as (3.13).

$$\delta = 0.37 \cdot x \cdot \left(\frac{U_e \cdot x}{\nu}\right)^{-\frac{1}{5}} \tag{3.13}$$

(3.13) gives quite accurate results (within 10%). In fact this correlation is used in [16]. However for boundary layer flows with pressure gradient, no such correlation exists. Therefore another way should be looked.

Boundary layer thickness is a rather vaguely defined parameter. Usual definition is the distance from the wall where the streamwise velocity reaches the 99% of its boundary layer edge value. This vague definition does not permit to make theoretical work on it and to find appropriate functions to calculate the δ. Therefore in this thesis work, boundary layer thickness is found from the computations iteratively. This is achieved in such an iterative procedure :

- δ is initialized using (3.13)
- The boundary layer equations are solved with this initial value of δ
- After the solution is complete, the distance from the wall for which streamwise velocity reaches the 99% of the edge velocity is calculated for each x location.
- With this new value of δ, the solution of the flowfield is repeated.
- The iterations are continued until a certain convergence is achieved.

The convergence of δ for each iteration is shown in Figure 3.10.

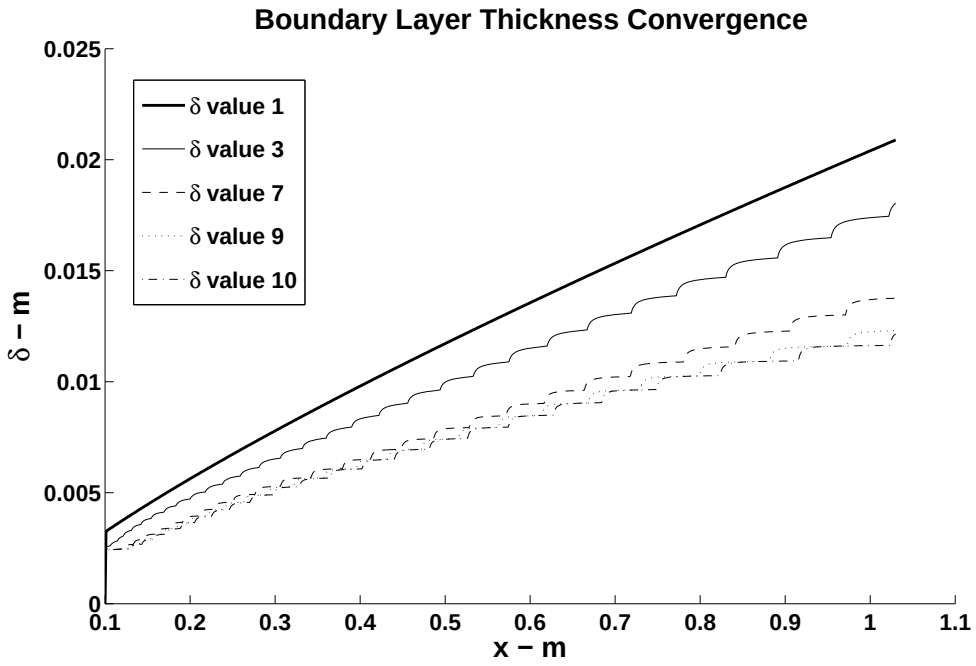

Figure 3.10: Convergence of δ for flat plate with zero pressure gradient ($U_\infty = 31m/s$, $\rho = 1.225kg/m^3$, $\nu = 1.58e-3$)

The convergence rate is quite good until about 0.1. However after this value, the convergence rate becomes very slow (Figure 3.11). Therefore the iterations

are finished when change in δ is less than 10%. However the accuracy of the calculations degrades with this relatively high convergence threshold. It is accurate within 30% when it is compared with experimental data.

With the convergence threshold value of 10%, convergence can be achieved within 10 iterations.

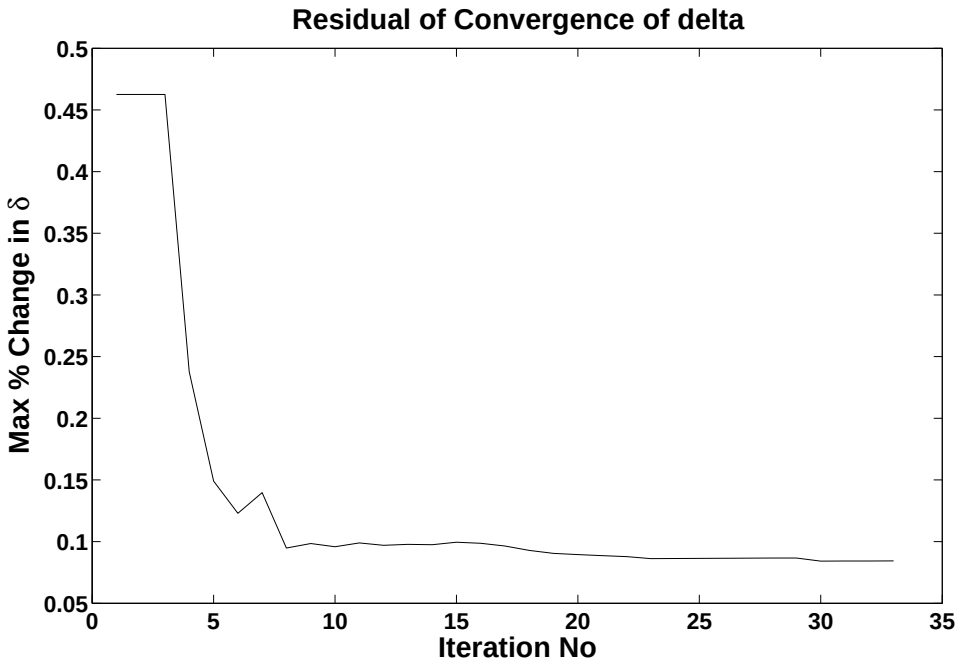

Figure 3.11: Maximum % Change in δ during the iterative solution ($U_\infty = 31m/s$, $\rho = 1.225kg/m^3$, $\nu = 1.58e-3$)

Calculation of Friction Velocity

Another parameter that should be supplied to the turbulence model is the friction velocity u_τ. The formal definition of u_τ is

$$u_\tau = \sqrt{\frac{\tau_{wall}}{\rho}} \tag{3.14}$$

Using the relation between the wall shear stress (τ_{wall}) wit the derivative of the velocity, an alternative form of (3.14) is given in (3.15).

$$\tau_{wall} = \rho\nu \left.\frac{\partial U}{\partial y}\right|_{y=0}$$
$$\Rightarrow u_\tau = \sqrt{\nu \left.\frac{\partial U}{\partial y}\right|_{y=0}} \tag{3.15}$$

However usage of (3.15) requires very fine grid near the wall and a very well behaving turbulence model near the wall. Furthermore since it requires a derivative calculation, the error in the streamwise velocity is amplified with this operation. Therefore an alternative method is sought.

The classical boundary layer equations are in differential form. With the integration of them, another exact relation can be achieved, which is called *Von Karman Momentum Integral Equation* ([9]), given in (3.16).

$$\frac{d\theta}{dx} + \frac{\theta}{U_e}\frac{dU_e}{dx}\left(H + 2 - M^2\right) = \left(\frac{\tau_{wall}}{\rho U_e^2}\right) \tag{3.16}$$

where

δ^* is the displacement thickness

$$\delta^* = \int_0^\delta \left(1 - \frac{U}{U_e}\right) dy$$

θ is the momentum (loss) thickness

$$\theta = \int_0^\delta \frac{U}{U_e}\left(1 - \frac{U}{U_e}\right) dy$$

H is the shape factor

$$H = \frac{\delta^*}{\theta}$$

(3.16) can be used with (3.14) in order to calculate u_τ.

(3.16) is an exact equation and it is related to the integral parameters of the boundary layer. Hence the accuracy of the turbulence model directly affects the calculations. Yet this might degrade the accuracy of the calculations, it also permits the ultimate accuracy of the model.

However there is a problem with the evaluation of (3.16). It requires the calculation of $d\theta/dx$. Momentum thickness is shown in Figure 3.12.

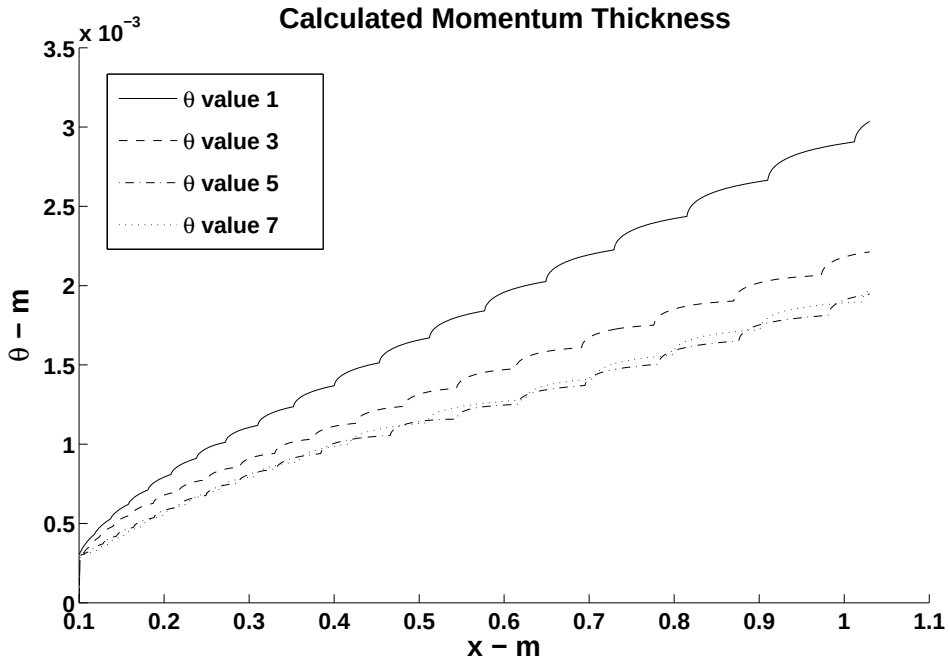

Figure 3.12: Calculated momentum thickness for flat plate with zero pressure gradient ($U_\infty = 31m/s$, $\rho = 1.225kg/m^3$, $\nu = 1.58e-3$)

As can be seen from 3.12, there is a low frequency wave like structure on the mean momentum thickness. For the calculation of the derivative, such a low frequency noise brings inaccurate results. The points within these wave like-structures can be up to 100. Therefore any practical order finite difference scheme fails to predict the derivative correctly. However there is advantage in the nu-

merical scheme. For the calculation of δ, the solution is made iteratively over the flowfield, as explained in the previous section. Therefore the whole momentum thickness profile is available after the each iteration and therefore all the points can be used to estimate the derivative at a given point. For this purpose, a fit can be made to the data. Usually polynomials are used for such fitting purposes. Since the coefficients of them are linear, they can be estimated in the least squares sense directly. However the purpose of the fit that is made is to estimate the derivative. Unfortunately there is a very huge drawback of fitting with polynomials. They are not good for derivative calculations and they can behave poorly as the boundaries of the fitting domain are approached, especially as the order of the polynomial is increased. It should be remarked that any zero or negative value of $d\theta/dx$ makes the system singular. Therefore fitting with polynomials is abandoned for a better fitting function.

It is interesting that most of the correlations for turbulence involves power laws. Therefore it is logical to use a fit in the form of a power law. Therefore a function in the form of,

$$\theta = A + B \cdot x^n$$

is used to fit the data. The problem with such a form is that its parameters have a nonlinear relation which does not permit a classical linear least squares fit. Instead, nonlinear optimization techniques should be applied ([4]).

The optimization problem is cast into following : Finding the optimum value of the parameters A, B, and n which makes the difference between the fit data and the fitting function minimum in the least squares sense. Gauss gradient search

algorithm is used in the solution, which is the simplest algorithm for nonlinear optimization and can be found in any textbook on nonlinear optimization.

The algorithm finds the optimum value iteratively and typical iteration number is 6 to 10. A typical fit to data using the nonlinear optimization technique is shown in Figure 3.13.

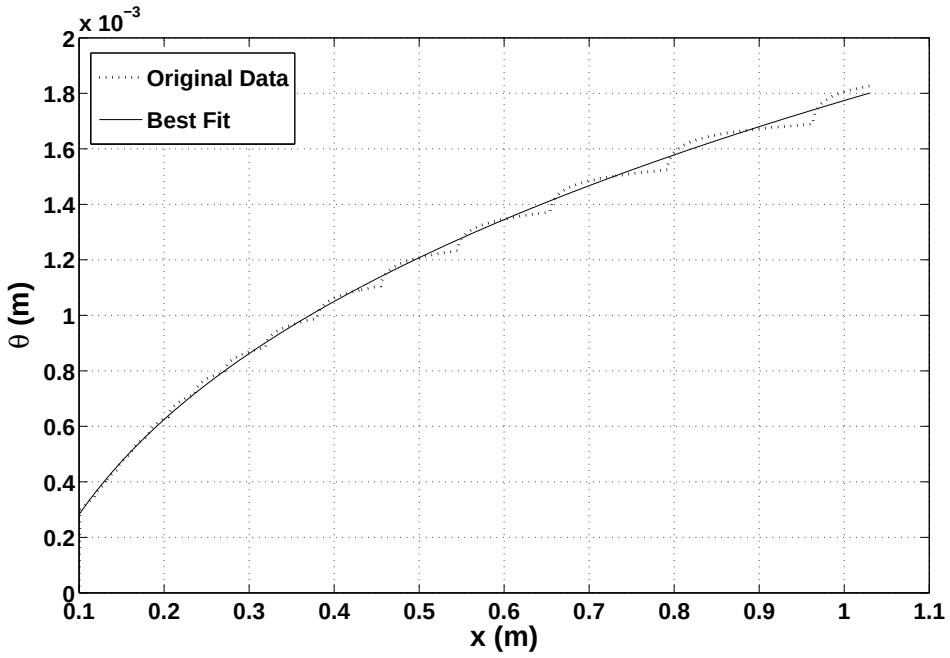

Figure 3.13: Calculated momentum thickness and best fit to the data with a function in the form of $\theta = A + B \cdot x^n$ ($U_\infty = 31m/s$, $\rho = 1.225kg/m^3$, $\nu = 1.58e-3$)

However fitting a function in the form of a power law is failed to give appropriate results for the boundary layers with pressure gradient. This is due to the disadvantage of the nonlinear least squares fit technique that it diverges if the fitting function is not chosen appropriately. Therefore classical polynomial fits are used for pressure gradient case. To avoid the erroneous behavior of the polynomial fits at the boundaries, various techniques are used (Like using weighted

least squares or smoothing the data etc.).

The calculation of u_τ with the above mentioned method necessities a priori knowledge about the solution of the flowfield. This is accomplished with the calculation of $d\theta/dx$ after the first iteration for δ. The initial u_τ is acquired using the correlation for flat plate ([24]) :

Near Wall Treatment

As explained in section 2.3 and section 3.1.2, the behavior of the model near the wall is not accurate in this might result in the divergence of the solutions from the actual solution. In order to inhibit this behavior, a correction is made at each step near the wall. This is done using the analytical solution of the boundary layer equations near the wall, i.e. Law of the Wall :

$$u^+ = \frac{1}{\kappa} \ln y^+ + B \qquad 30 < y^+ < 100 \sim 1000$$

$$u^+ = y^+ \qquad y^+ < 5$$

The correction is made in the following sense.

- Between $30 < y^+ < 100$, a point is sought for which the difference between the theoretical velocity profile (from Law of the Wall) and the calculation is minimum.

- This point is chosen to be the correction point

- The velocity profile is fit to data between the correction point and the wall

- The fitting is done using cubic splines. The boundary conditions at the wall is taken as $U = 0$ and $dU/dy = u_\tau^2/\nu$

The correction point usually lies very close to $y^+ = 30$.

This correction might give a false impression that the performance of the model is artificially improved. But this is not true since both the u_τ and the U and dU/dy values used for fitting is supplied by the model. Therefore this correction directly depends on the performance of the model. It might seen as a replacement for a wall function.

3.2 Grid Generation

The grid generation is one of the specific issues of computational fluid dynamics and many sources exists for this problem. Fortunately, since the numerical solution algorithm for the equations under interest is a marching type and the solution in x direction and y direction is uncoupled. Therefore two 1-Dimensional girds, one for x and one for y will be sufficient. Furthermore the geometry is the simplest type : Flat Plate. Hence, a rectangular, cartesian grid system will be sufficient for the purpose of this work.

Generally, the grid generation algorithm boils down to solution of 2^{nd} order differential equations whose solutions are 1-Dimensional grids with a specified length. The class of these 2^{nd} order differential equations gives the name of the grids, like *hyperbolic*, *parabolic* etc. ([25]). The classification is done according to the method explained in section 3.1.

The technique used for the generation of the grids is finding a transformation

to map the solution of the grid differential equation to a an equally spaced points in the interval $[0, 1]$. The spacing of the solution is adjusted using a weighting function P. Therefore mathematically, the grid generation boils down to finding a transformation having P as the parameter with guaranteing that the Jacobian of the transformation $J > 0$.

Specifying P is usually done using a stretching function. Stretching functions are used to generate grids in the $x_1 = 0, x_2, \ldots x_i \ldots x_n = 1$ interval and then the generated grids (x) are transformed into the actual grids (y) using :

$$y = y_{min} + (y_{max} - y_{min}) \cdot x$$

Three most common used stretching forms are explained below :

Geometric Progression In this method, the grid spacing at node i is given by

$$x_{i+1} - x_i = \alpha \cdot (x_i - x_{i-1}) \Rightarrow x_i = \frac{\alpha^{i-1} - 1}{\alpha^n - 1}$$

or with defining a uniform spacing variable $u = \frac{i-1}{n-1}$, grid point at any u can be formulated as :

$$x(u) = \frac{\alpha^{(n-1)\cdot u} - 1}{\alpha^{n-1} - 1}$$

α is the stretching parameter and should be explicitly defined.

Exponential Stretching With the definition of uniform spacing variable, u, the grid point at any u can be formulated as :

$$x(u) = \frac{e^{\beta \cdot u} - 1}{e^{\beta} - 1}$$

β is the stretching parameter and should be explicitly defined.

Hyperbolic Tangent Stretching With the definition of uniform spacing variable, u, the grid point at any u can be formulated as :

$$x(u) = 1 + \frac{\tanh\left(u-1\right)\cdot\frac{\delta}{2}}{\tanh\frac{\delta}{2}}$$

δ is the stretching parameter and should be explicitly defined.

In each stretching method, a stretching parameter that should be defined, exists. However, in the solution of fluid mechanics problems, arbitrarily defining a non-physical parameter has not much of a use. It is more appropriate to define the spacing between the first two grid points since, especially for the turbulence calculations, it represents the minimum distance from the wall and it has a vital importance for resolving the boundary layer sub-layers properly. For this purpose, a methodology for the specification of the stretching parameter from the spacing between the first two grid points is developed for each method. The details are as follows:

For the numerical solution of boundary layer flows, the first grid point is taken at the wall. Therefore $y_{min} = y_1 = 0$. The distance of the second grid point from the wall can be can be formulated as $dy = y_2 - y_1 = y_2$. Let y_{max} be the maximum distance from the wall, then $dx = x_2 - x_1 = x_2 = x(u = \frac{1}{n-1})$ can be formulated as,

$$dx = \frac{dy}{y_{max}}$$

With this definition of dx and the specify the total number of grid points (n), stretching parameters can calculated.

Geometric Progression For geometric progression technique, α can be formulated as:

$$dx = x_{i=2} = \frac{\alpha - 1}{\alpha^n - 1}$$

$$\Rightarrow \qquad \alpha^n - \frac{1}{dx} + \left(\frac{1}{dx} - 1\right) = 0$$

This equation can be solved using Newton-Raphson method ([17]). But the desired accumulation of the grid points near the wall does not satisfied with lower n values. Since increasing n results in increase of computational time, this method had not been preferred.

Exponential Stretching For exponential stretching technique, β can be formulated as:

$$dx = \frac{e^{\beta \cdot \left(\frac{1}{n-1}\right)} - 1}{e^{\beta} - 1}$$

$$\beta' = e^{\beta} \qquad \Leftrightarrow \qquad \beta = \ln \beta'$$

$$\Rightarrow \qquad \beta' - \frac{1}{dx} \cdot \beta'^{\frac{1}{n-1}} + \left(\frac{1}{dx} - 1\right) = 0$$

This equation can be solved using Newton-Raphson method ([17]). However the solutions usually does not converge for desired dy and n parameters.

Hyperbolic Tangent Stretching For hyperbolic tangent stretching technique, δ can be formulated as:

$$dx = 1 + \frac{\tanh\left(\frac{\delta}{2} \cdot \frac{2-n}{n-1}\right)}{\tanh\frac{\delta}{2}}$$

$$\Rightarrow \qquad (dx - 1) \cdot \tanh\frac{\delta}{2} - \tanh\left(\frac{\delta}{2} \cdot \frac{2-n}{n-1}\right) = 0$$

This equation can be solved using Newton-Raphson method ([17]).

The above mentioned methods can be used both for grids of x and y directions. However, stretching is more critical for the y grid. Therefore stretching is used for only the y grid. For the x grid, grid with equally spaced points is used.

Although all three of the grid generation algorithms are implemented into the program, *Hyperbolic Tangent Stretching* method is used in the calculations. The number of grid points (n) is usually taken as 50-75 and the distance of the second grid from the wall is taken according to the flow conditions with satisfying $y^+ = 3 - 5$.

The grid independence of the solutions is explained in section 4.1.

3.3 Numerical Solution Scheme

The integration of streamwise and wall normal velocity can be executed using the methods described in section 3.1. But the order of the execution of the operations differs the accuracy of the results. Therefore the exact execution order is given below for convenience.

The solution scheme starts with the generation of the U profile at the first x location, i.e. $U(x_0, y)$

For each x location ($x_j = x_j - 1 + dx$), $V^1(x_j, y)$ is calculated using (3.7) with $U(x_{j-1}, y)$. Heun's method is used in the calculations :

$$
\begin{aligned}
V|_{1,k} &= 0 \\
\\
\frac{\partial V^1}{\partial y} &= \frac{\frac{\partial U}{\partial y}\Big|_{j,k-1}}{U|_{j,k-1}} \cdot V|_{j-1,k} + \frac{1}{\rho} \cdot \frac{dP}{dx}\Big|_k - \frac{\nu}{U|_{j,k-1} \cdot \rho} \cdot \frac{\partial^2 U}{\partial y^2}\Big|_{j,k-1} \\
&- \frac{1}{U|_{j,k-1} \cdot \rho} \cdot \frac{\partial \tau}{\partial y}\Big|_{j,k-1} \\
V^1 &= V|_{j-1,k} + \frac{\partial V^1}{\partial y} \cdot \left(y|_j - y|_{j-1} \right) \\
\frac{\partial V^2}{\partial y} &= \frac{\frac{\partial U}{\partial y}\Big|_{j,k-1}}{U|_{j,k-1}} \cdot V^1 + \frac{1}{\rho} \cdot \frac{dP}{dx}\Big|_k - \frac{\nu}{U|_{j,k-1} \cdot \rho} \cdot \frac{\partial^2 U}{\partial y^2}\Big|_{j,k-1} \\
&- \frac{1}{U|_{j,k-1} \cdot \rho} \cdot \frac{\partial \tau}{\partial y}\Big|_{j,k-1} \\
\frac{\partial V'}{\partial y}\Big|_{j,k} &= \frac{1}{2} \cdot \left(\frac{\partial V^1}{\partial y} + \frac{\partial V^2}{\partial y} \right) \\
V^1\Big|_{j,k} &= V|_{j-1,k} + \frac{\partial V'}{\partial y}\Big|_{j,k} \cdot \left(y|_j - y|_{j-1} \right)
\end{aligned}
$$

With the calculation of $V^1(x_j, y)$, $\frac{\partial V'}{\partial y}(x_j, k)$ is automatically generated and $\frac{\partial U'}{\partial x}(x_j, k)$ can be calculated using the continuity equation, (3.11) and with the

integration of it, $U^1(x_j, y)$ can be generated :

$$U^1\Big|_{j,k} = U|_{j,k-1} \underbrace{- V'|_{j-1,k}}_{=\frac{\partial U}{\partial x}} \cdot \Big(x|_k - x|_{k-1}\Big)$$

This result can be used in V calculations to get an updated V profile :

$$\begin{aligned}
V|_{1,k} &= 0 \\
\\
\frac{\partial V^1}{\partial y} &= \frac{\frac{\partial U^1}{\partial y}\Big|_{j,k-1}}{U^1|_{j,k-1}} \cdot V|_{j-1,k} + \frac{1}{\rho} \cdot \frac{dP}{dx}\Big|_k - \frac{\nu}{U^1|_{j,k-1} \cdot \rho} \cdot \frac{\partial^2 U^1}{\partial y^2}\Big|_{j,k-1} \\
&- \frac{1}{U^1|_{j,k-1} \cdot \rho} \cdot \frac{\partial \tau}{\partial y}\Big|_{j,k-1} \\
V^1 &= V|_{j-1,k} + \frac{\partial V^1}{\partial y} \cdot \Big(y|_j - y|_{j-1}\Big) \\
\frac{\partial V^2}{\partial y} &= \frac{\frac{\partial U^1}{\partial y}\Big|_{j,k-1}}{U^1|_{j,k-1}} \cdot V^1 + \frac{1}{\rho} \cdot \frac{dP}{dx}\Big|_k - \frac{\nu}{U^1|_{j,k-1} \cdot \rho} \cdot \frac{\partial^2 U^1}{\partial y^2}\Big|_{j,k-1} \\
&- \frac{1}{U^1|_{j,k-1} \cdot \rho} \cdot \frac{\partial \tau}{\partial y}\Big|_{j,k-1} \\
\frac{\partial V}{\partial y}\Big|_{j,k} &= \frac{1}{2} \cdot \left(\frac{\partial V^1}{\partial y} + \frac{\partial V^2}{\partial y}\right) \\
V|_{j,k} &= V|_{j-1,k} + \frac{\partial V}{\partial y}\Big|_{j,k} \cdot \Big(y|_j - y|_{j-1}\Big)
\end{aligned}$$

With this updated V profile, $U(j,k)$ can be calculated, as before, with,

$$U|_{j,k} = U|_{j,k-1} \underbrace{- V|_{j-1,k}}_{=\frac{\partial U}{\partial x}} \cdot \Big(x|_k - x|_{k-1}\Big)$$

Calculation of Derivatives

The solution of the boundary layer equations with the above mentioned methodology requires the calculation of first and second order derivatives. But since the

solution procedure is not iterative, derivative calculations can be made explicitly, ones the velocity profiles are generated and therefore any order of accuracy finite difference formulas can be used. However there is a problem with the spacing of grids. For grid in x direction, there is no problem at all since the grid points are equally spaced and this value can be used in the finite difference formulation directly. However, for stretched grid of y direction, it is not easy to implement the grid spacings into the formulation, especially for higher order schemes. To overcome this problem, grid of y direction is transformed into a computational domain where the space between the grid points become unity.

Let η represent the coordinates in the computational domain and let y be the grids in the physical domain. Then ∂_η can be written as ([21]) :

$$\partial_y = \eta_y \cdot \partial_\eta \tag{3.17}$$

However, η_y can not be calculated easily using finite difference formulations because the y points are not equally spaced. But instead, (3.17) can be written in the reverse sense :

$$\partial_\eta = y_\eta \cdot \partial_y \tag{3.18}$$

Equating (3.17) and (3.18) results in,

$$\eta_y = \frac{1}{y_\eta}$$

and y_η can be calculated easily using any order finite difference formulation since η are equally spaced.

In the calculations, second order backward and forward difference schemes

are used for the grid points at the boundaries and second order central difference scheme is used for the mid-points ([14]).

After the transformation of the grid points, the derivatives can be calculated using;

$$\begin{aligned} \partial_y &= \eta_y \cdot \partial_\eta \\ \partial_y^2 &= \eta_y^2 \cdot \partial_\eta^2 \end{aligned}$$

For the calculation of ∂_η and $\partial^2\eta$, any order finite difference formulation can be used since η are equally spaced. In the calculations, second order backward and forward difference schemes are used for the grid points at the boundaries and second order central difference scheme is used for the mid-points ([14]).

As mentioned above, the transformation of x grid points is generally not necessary. However at some circumstances, for example for the taking of $\frac{dP}{dx}$ derivative from experimental pressure measurements at different x locations, it might be required to transform the x coordinates also. This is done by calculating x_ξ and ξ_x metrics, similar to the formulations given in (3.17) and (3.18).

3.4 The Programming Language

For the numerical solution of fluid dynamics problems, *FORTRAN* programming language dominates fluid dynamics community since beginning of this research field. Although new languages like *C++* or *Java* are emerging as a programming tool, *FORTRAN* is still the preferred with its smaller execution time and performance. However, as with all of the pre-compiled languages, *FORTRAN* brings all the drawbacks of the high level programming languages: The program

should be compiled before execution, only selected variables are available after the execution ends and the results can only be taken from the screen directly or from an external file. These results should be analyzed and visualized with other programmes. If a single solution is needed, these steps (can be called as post-processing) are not comparable to computational efficiency of the language. However for development purposes, post-processing takes much more time than the execution time.

The program developed for this thesis is a development tool for turbulence model. Therefore a program whose solutions can be directly seen after the execution of the program, in which quick calculations for the verification can be easily done and where all of the variables are available after the executions are done would be very useful. One such platform is *MATLAB*. *MATLAB* does not compile the programme and the execute it line by line. This significantly increases the computational time for iterative processes. However *MATLAB* has a countermeasure for this problem. The long name for *MATLAB* is "MATrix LABoratory". It has its own optimization methods for the execution of matrix operations and it significantly reduces the execution time if operations are written in matrix form rather than in "for loops". With keeping in mind this property of *MATLAB* during the programming, the execution times comparable to *FORTRAN* can be achieved.

After their pros and cons are carefully weighted, *MATLAB* is chosen to be the programming language for the developed program. The typical execution times of the program is given Table 3.4, for a standard laptop PC with Intel Pentium 4

Table 3.2: The average execution time of the program for a single solution

	x_{max} (m)	y_{max} (m)	Number of Grid Points in x Direction	Number of Grid Points in y Direction	Execution Time (sec)
1	1.03	0.05	931	50	9.075
2	1.03	0.05	931	75	11.081
3	4.12	0.05	4115	50	41.734

processor, 2.6 GHz speed and 256 megabyte RAM.

CHAPTER 4

RESULTS

4.1 Solution over a Flat Plate

As usual in the validation of turbulence models, the investigation of the models performance will be started with the simplest case of flow over a flat plate. Actually the models validation against the flat plate is accomplished previously in [16]. However the current work diverges from [16] in the following sense. The calculations in [16] involved the calculation of δ and u_τ from correlations given in Chapter 3. However, as explained in Chapter 3, the current work involves the calculation of these parameters from the solution itself. Therefore the results presented in this section represents the ultimate performance of the model.

The model's performance will be compared with the experimental results taken from [1]. The experiment conditions are given Table 4.1.

The flow conditions are simulated with the data given in Table 4.1. The results are summarized below.

Table 4.1: The experimental conditions for the flat plate without pressure gradient

x (mm)	Re_θ	U_∞ (m/s)	u_τ (m/s)	δ (mm)	δ^* (mm)	θ (mm)	H
1.021	5021	32.85	1.236	19.29	3.33	2.4	1.39
4.124	13052	33.04	1.17	54.98	8.13	6.22	1.31

For the experimental condition for $x = 1.021$, the calculated and the experimentally measured values of streamwise velocity is given Figure 4.1 and the percent error is given in Figure 4.2.

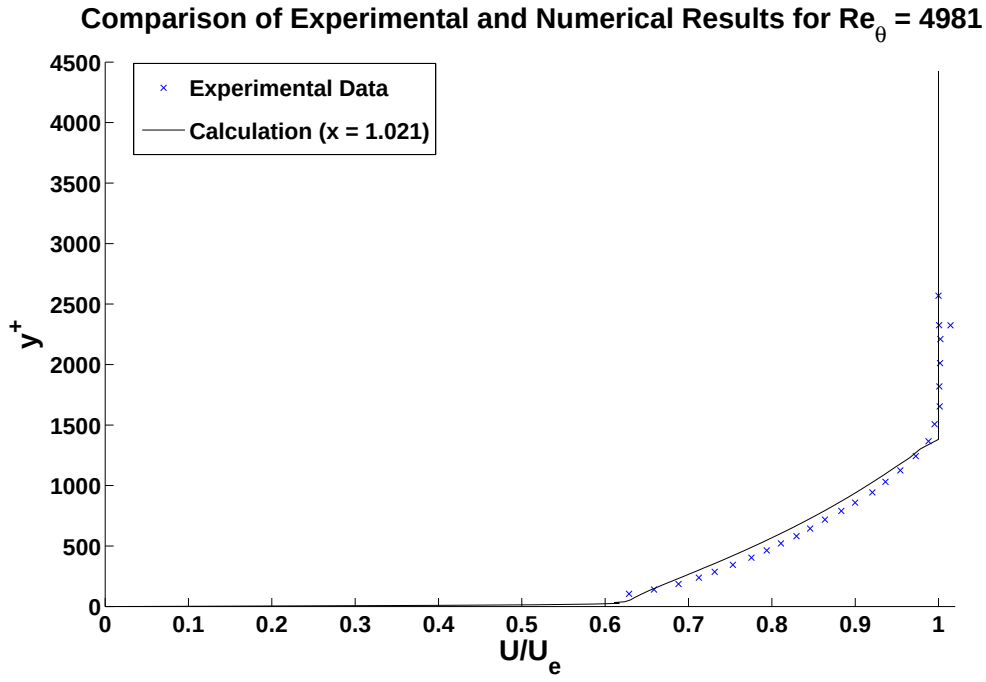

Figure 4.1: Comparison of experimentally measured and computed velocity profiles for Zero Pressure Boundary Layer for $x = 1.021$

As can be seen from Figure 4.1 and Figure 4.2, the error between computations is on the order of 3%. However the error is cumulated at the near wall and the boundary layer edge region. Therefore it seems that the error at near wall region is due to the error in the calculation of u_τ and the error at the boundary layer edge is due to the error in the calculation δ. These errors led to a 3% error

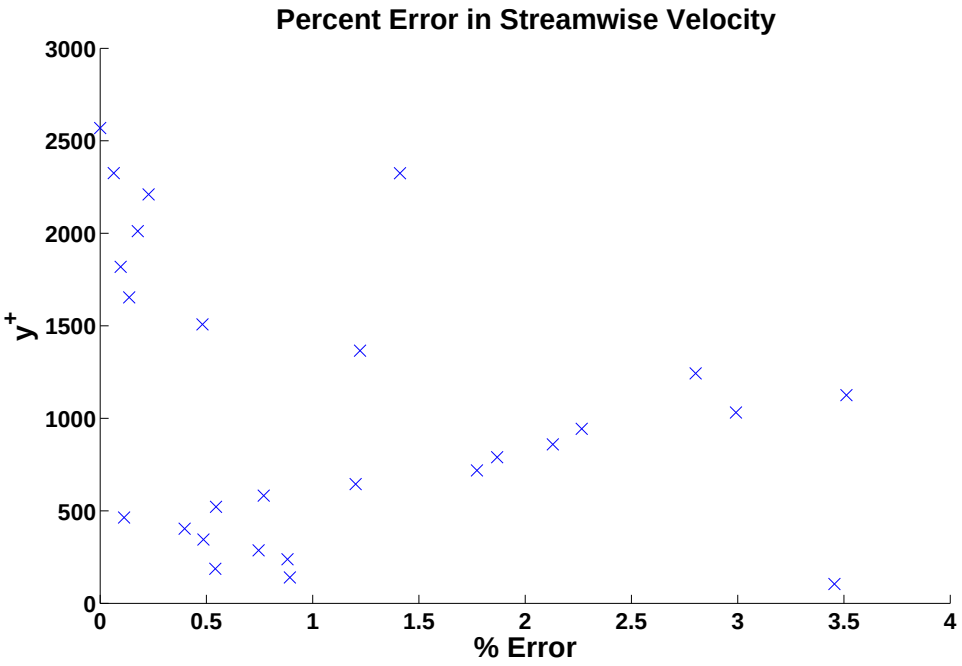

Figure 4.2: Percent error with the experimentally measured and computed velocity profiles for Zero Pressure Boundary Layer for $x = 1.021$

in the calculations. Actually the error in the calculations are reduced to 2% if flat plate correlations are used in the δ and u_τ calculations (Figure 4.3). Therefore it is believed that the error can be reduced with an improved wall treatment and with an improvement on the δ calculation.

It is appropriate now to discuss the grid independence of the solutions. The computed velocity profiles with grid numbers of 50 and 75 are shown in Figure 4.4. The difference between them is on the order of 8%.

As can be seen from Figure 4.4 that the majority of this discrepancy comes from the error in δ calculations. In fact if the same δ is used in the calculations, the discrepancy reduces to less than 5%. The comparison is shown in Figure 4.5.

The results for the $x = 4.124$ are shown in Figure 4.6 and Figure 4.7.

Similar comments can be made for the $x = 4.124$ case. However the error

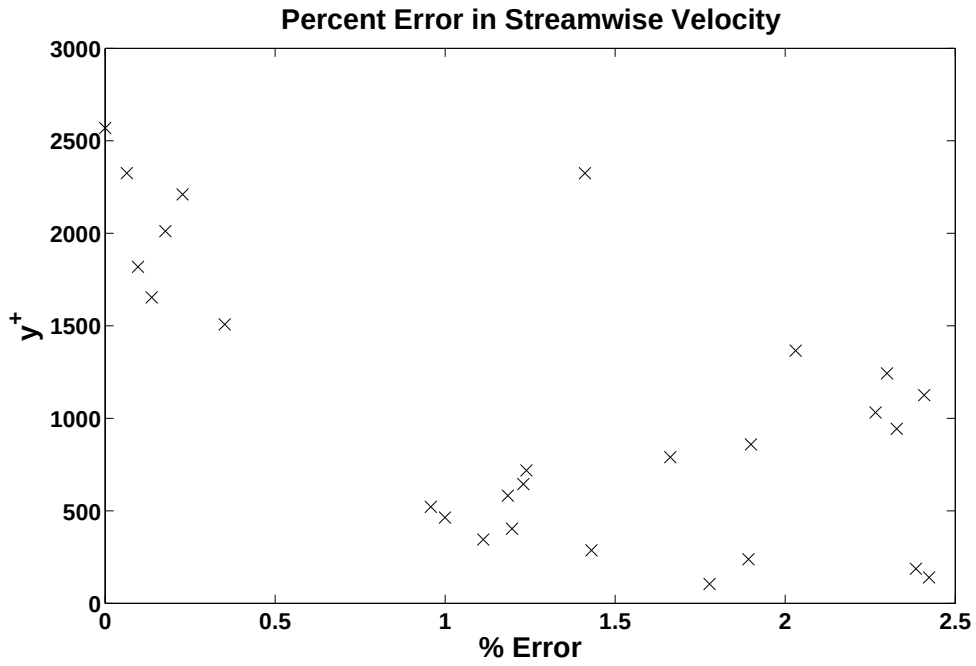

Figure 4.3: Percent error with the experimentally measured and computed velocity profiles for Zero Pressure Boundary Layer for $x = 1.021$ (Flat plate correlations are used for δ and u_τ calculations)

is increased to 11%. This increase is the result of the x marching structure of the solution scheme. The error is amplified while solution is generated in the x direction.

Finally, the comparison of integral parameters are given in Table 4.2.

Table 4.2: The comparison of experimental data for the flat plate without pressure gradient with computations

	x (mm)	u_τ (m/s)	δ (mm)	θ (mm)	H
Experimental Measurement	1.021	1.236	19.29	2.4	1.39
Calculation	1.021	1.4	15.4	2.1	1.37
Experimental Measurement	4.124	1.17	54.98	6.22	1.31
Calculation	4.124	0.811	34.8	1.14	1.33

Table 4.2 indicates that integral parameters of the boundary layer can not be computed accurately (the error is on the order of 15%), which results in calcu-

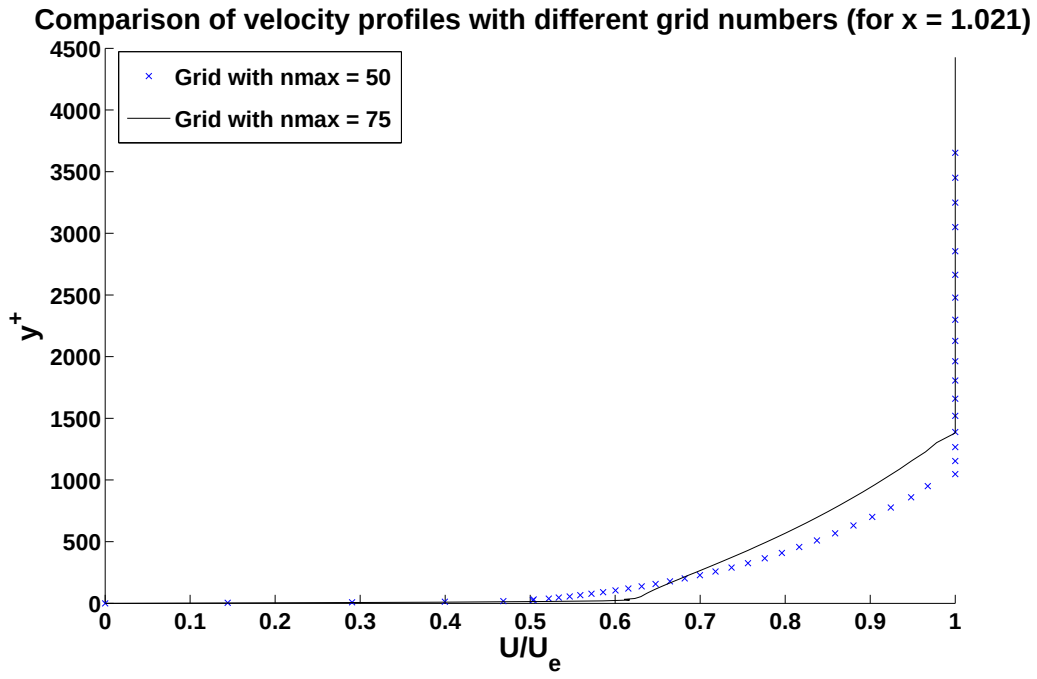

Figure 4.4: Comparison of computed velocity profiles with different grid numbers for Zero Pressure Boundary Layer for $x = 1.021$

lation of u_τ inaccurately which degrades the accuracy of the velocity field calculations. Actually it is a common problem in most of the turbulence models that they can not represent the integral quantities. The difference of the current work is that integral parameters are fed back to flowfield calculations. However this is due to the solution scheme and is not related to turbulence model's performance. Therefore it is believed that the accuracy of solutions will be improved if a more advanced solution scheme is used.

4.2 Solution over a Flat Plate with Favorable Pressure Gradient

The second type of boundary layers that will be investigated is flow over a flat plate with favorable pressure gradient. Unfortunately there are not much data,

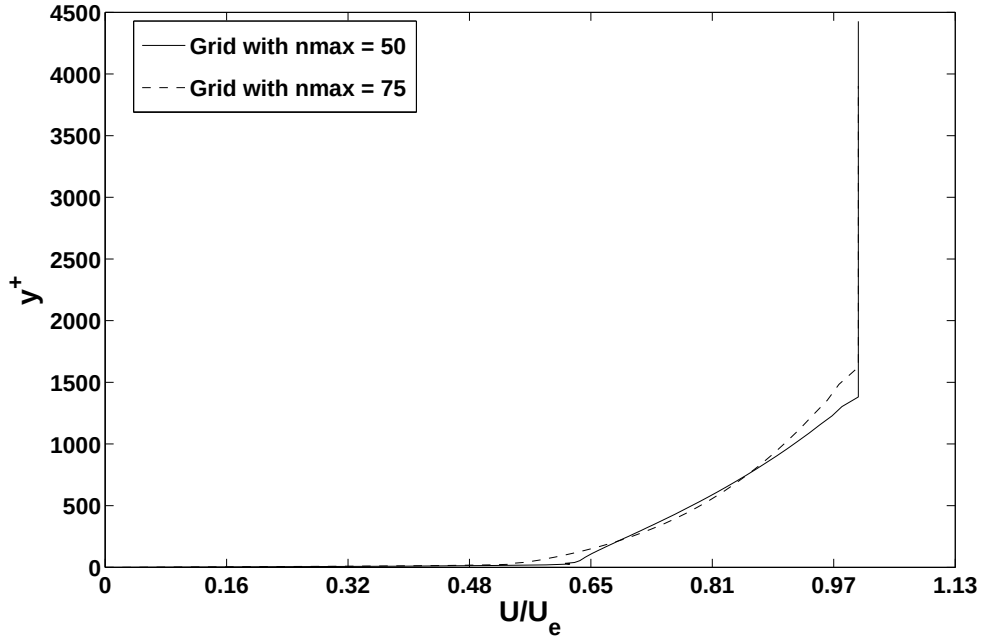

Figure 4.5: Comparison of computed velocity profiles with different grid numbers for Zero Pressure Boundary Layer for $x = 1.021$ (Flat plate correlations are used for δ calculations)

on favorable pressure gradient boundary layers, present in the open literature. Therefore a relatively old one will be used to verify the turbulence model. The experimental data that will be used is from 1968 Stanford Conference. The test case can be found in [11] as the case with flow identification number of 1300.

The data consists of measurements at various stations over the flat plate. Unfortunately the freestream conditions are unknown and the velocity measurements are taken only at the stations given in the data. The main flow parameters available are given in Table 4.3. Mean velocity is also available at various y locations at each station point.

As can be seen from Table 4.3, the initial station for the available data is at $x = 0.782\ m$ and the external velocity has a nonzero derivative at this station.

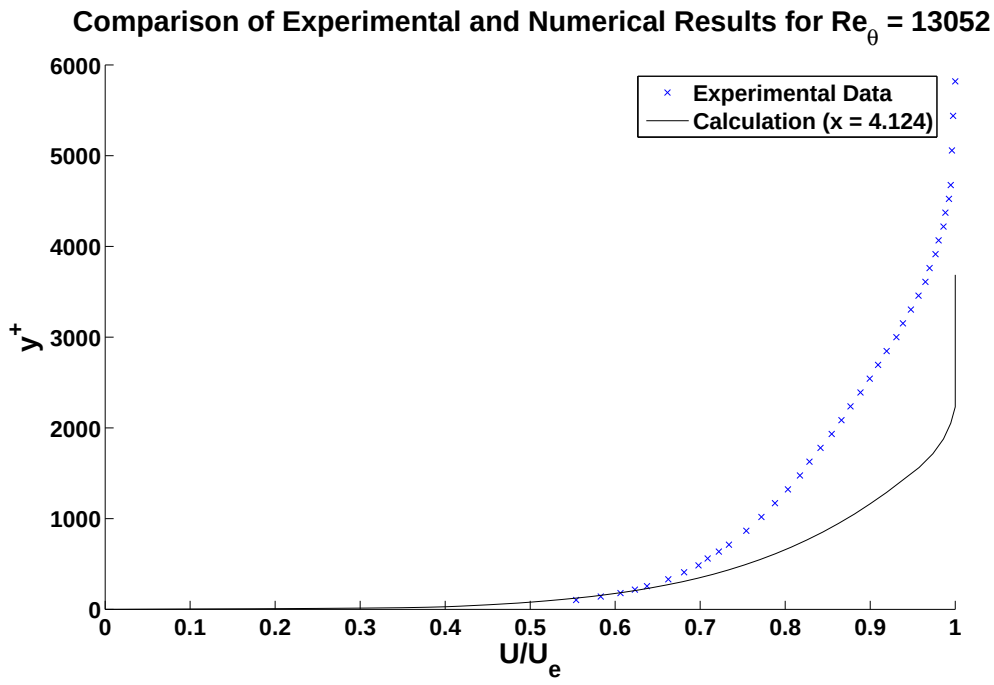

Figure 4.6: Comparison of experimentally measured and computed velocity profiles for Zero Pressure Boundary Layer for $x = 4.124$

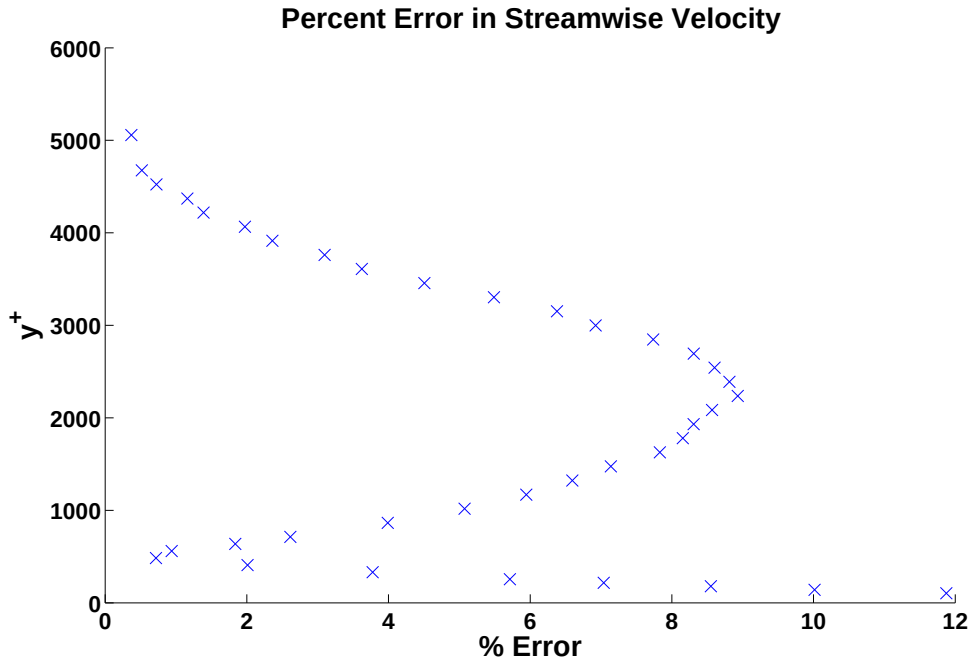

Figure 4.7: Percent error with the experimentally measured and computed velocity profiles for Zero Pressure Boundary Layer for for $x = 4.124$

Table 4.3: The main flow parameters for the flat plate with favorable pressure gradient for the experimental data taken from [11]

x (m)	U_e (m/s)	dU_e/dx $(1/s)$	θ (cm)	H	c_f
0.782	11.52	3.65	0.135	1.426	0.00454
1.282	13.38	4	0.149	1.376	0.00434
1.782	15.61	4.33	0.158	1.371	0.00415
2.282	17.85	4.68	0.173	1.36	0.00396
2.782	20.2	4.9	0.189	1.368	0.00365
3.132	22.07	5	0.196	1.363	0.00356
3.332	22.9	5	0.196	1.355	0.00347
3.532	23.7	4.96	0.203	1.347	0.00342
3.732	25.13	4.86	0.196	1.336	0.00348
3.932	25.8	4.6	0.219	1.353	0.00336
4.132	26.4	4.13	0.227	1.346	0.0033
4.332	27.5	3.5	0.227	1.341	0.0032

Therefore it can not be assumed that the flow is started from a zero pressure gradient flow at the leading edge. However, since the solution procedure is step marching method, an initial velocity profile is required for the numerical solver. It can be argued that the measurements in the initial station can be used as the initial profile. However the resolution of the measurements are not fine enough to be used as the initial profile. Therefore an alternative approach is taken.

From the experimental measurements, the external velocity, friction coefficient and the boundary layer thickness is available [1]. The x location at which a flat plate flow under zero pressure gradient has the same boundary layer thickness can be calculated using the correlation for flat plate :

$$\delta = 0.37 \cdot x \cdot \left(\frac{U_\infty x}{\nu}\right)^{-\frac{1}{5}}$$

The U_∞ value is taken as the external velocity at the first measurement station. x can be found as $x = 0.535\ m$. For this x location, friction velocity can be

[1] Boundary layer thickness is not among the parameters given in Table 4.3. However it can be calculated from the mean velocity data which is also supplied as a part of the experimental data.

calculated using the correlation for flat plate :

$$u_\tau = U_\infty \sqrt{0.0225 \left(\frac{\nu}{U_\infty \cdot \delta} \right)^{\frac{1}{4}}}$$

The error in the calculated friction velocity relative to the experimental measurement is less than 2%. The comparison of the computed velocity profile at the $x = 0.535\ m$ location and the experimentally measured velocity profile at the first measurement station is shown in Figure 4.8.

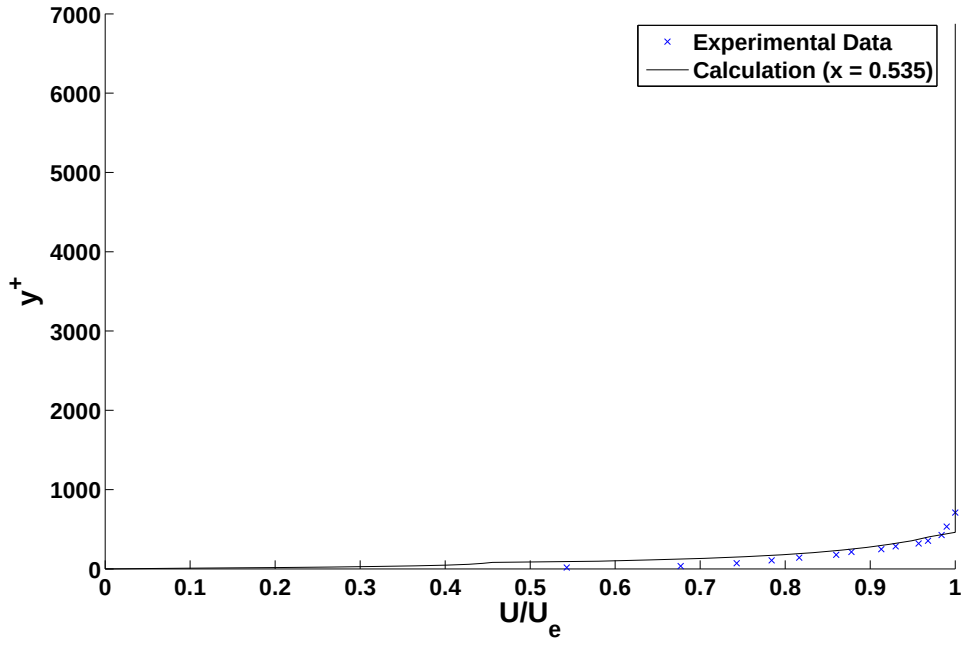

Figure 4.8: Comparison of the computed velocity profile at the $x = 0.535\ m$ location for a flat plate with zero pressure gradient and the experimentally measured velocity profile at the first measurement station

Therefore the numerical calculation can be done equivalently, on a flat plate, having the external velocity at the first measurement location as the freestream velocity and starting with zero pressure gradient until the $x = 0.535\ m$ location is reached. After this point, the pressure gradient observed in the experiment can be applied to the flow. It should be remarked that the experimental points

should be shifted by $-0.247\ m$ for the comparison with numerical results. All the comparisons given in this section are done after this shift.

Calculation of the pressure coefficient is another problem about the test case. The effect of pressure gradient is measured in terms of the external velocity gradient dU_e/dx. This term can be used to calculate the pressure gradient. From the Bernoulli equation, the pressure gradient can be written in terms of the external velocity as ([22]),

$$\frac{dP}{dx} = -\rho U_e \frac{dU_e}{dx}$$

Pressure gradient can be directly calculated from the experimental data using this equation. However to achieve the pressure (or equivalently, the pressure coefficient) at each x location, the calculated pressure gradient should be integrated. However the large distances between the measurement stations decreases the numerical accuracy of the calculations. To improve the numerical accuracy, the integration is done in this manner : The calculated pressure gradients are interpolated using spline functions over the grid in x direction. Then for each grid point, a second order polynomial is fitted to the grid point and the two adjacent points. The integration is done analytically with the fitted polynomial. Since the flow is started as a zero pressure gradient flow, the initial pressure coefficient can be taken as 0. The pressure coefficient used in the calculations is shown in Figure 4.9.

The comparison of the computed and experimentally measured velocity profiles for $x = 2.535\ m$ is shown in Figure 4.10. The error between the measurement and the computation is shown in Figure 4.11. As can be seen from Figure 4.11,

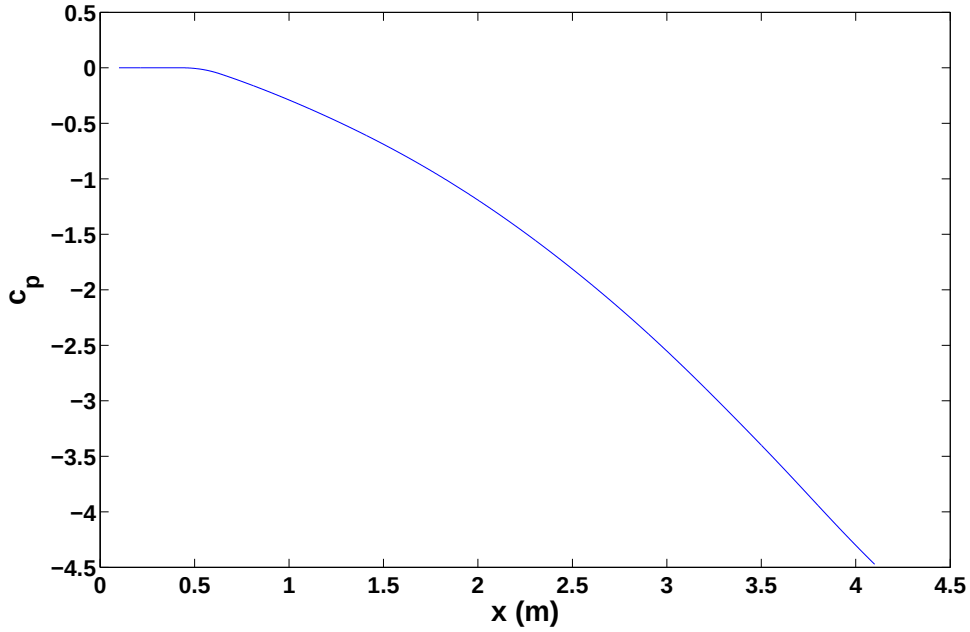

Figure 4.9: The pressure coefficient used in the calculation of favorable pressure gradient test case

the maximum error is less than 4% and the error is approximately equal at each y location. However as can be seen from the velocity profile, there is an error in the boundary layer thickness and the edge velocity predictions. The source of the error in the boundary layer thickness calculations is the solution methodology, as in the case of flat plate with zero pressure gradient case. The source of the error in the edge velocity is the numerical integration error made in the calculation of pressure coefficient. It can be claimed that the error can be reduced to the flat plate without pressure gradient case error level (on the order of 2 %) if these parameters can be predicted more accurately.

The comparison of the computed and experimentally measured velocity profiles for $x = 4.085\ m$ is shown in Figure 4.12. The error between the measurement and the computation is shown in Figure 4.13. For $x = 4.085\ m$, the error is in-

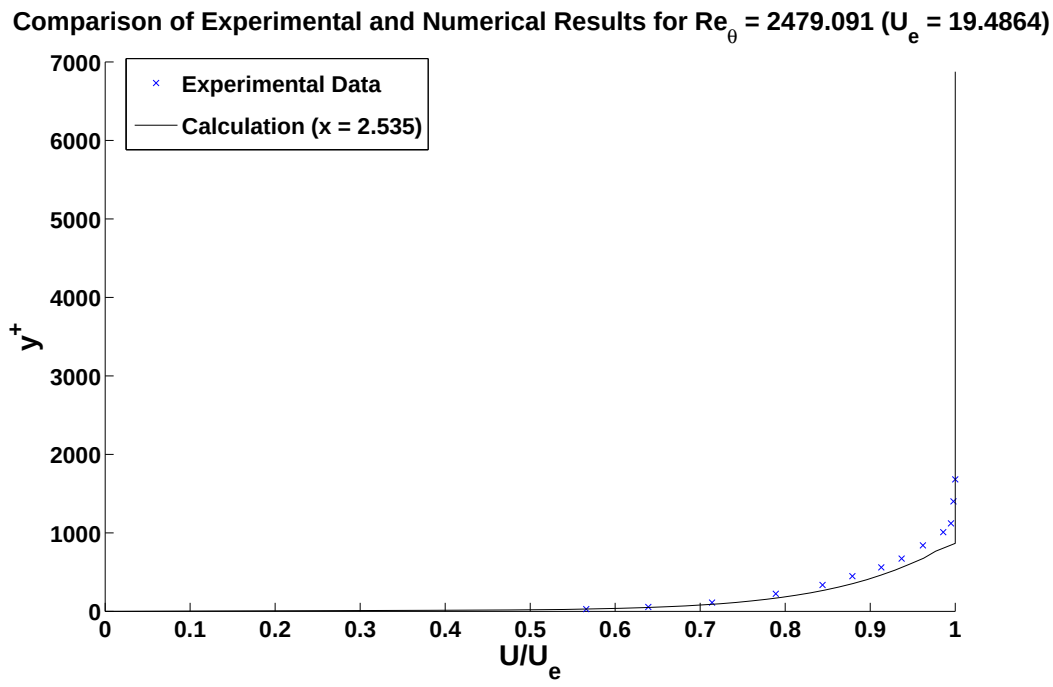

Figure 4.10: Comparison of experimentally measured and computed velocity profiles for Favorable Pressure Boundary Layer for $x = 2.535m$

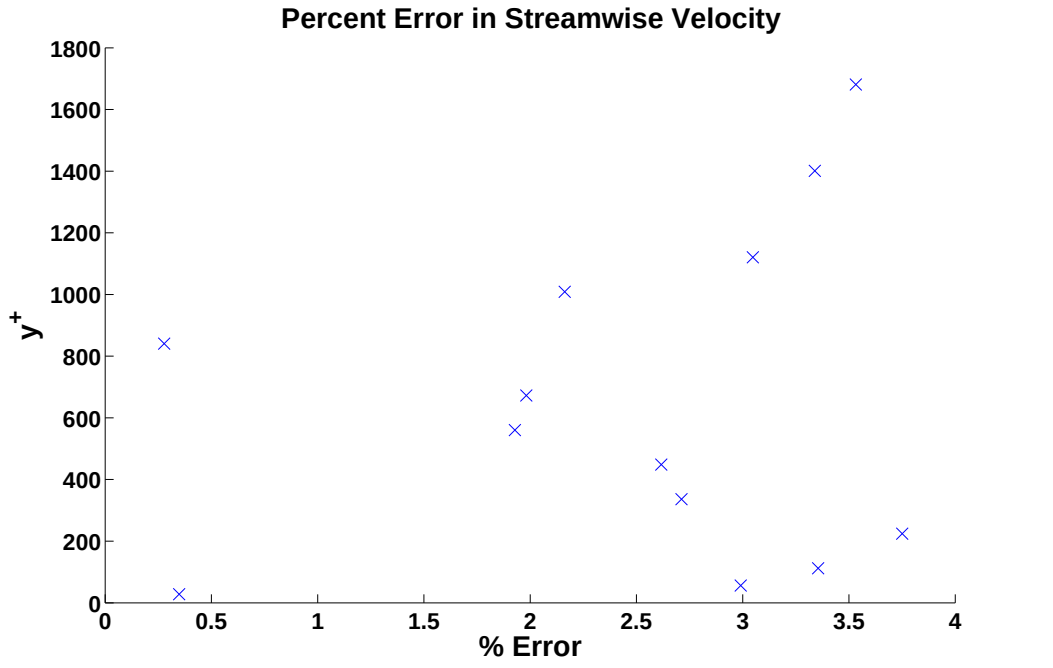

Figure 4.11: Percent error with the experimentally measured and computed velocity profiles for Favorable Pressure Boundary Layer for for $x = 2.535m$

creased to 7.5% level. The increase in the error is not unexpected since the error increases with the distance from the leading edge, due to the nature of the solution methodology. As can be seen from Figure 4.12, similar errors, in the prediction of the boundary layer thickness and the edge velocity, to the $x = 2.535\ m$ solution is present.

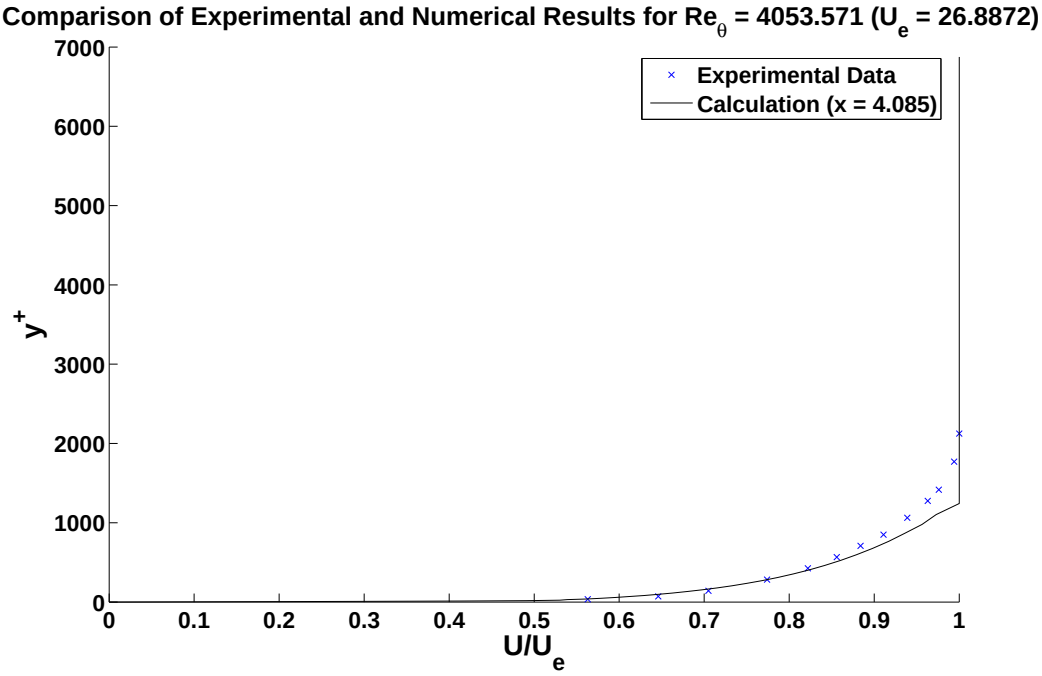

Figure 4.12: Comparison of experimentally measured and computed velocity profiles for Favorable Pressure Boundary Layer for $x = 4.085m$

Finally, the comparison of the integral parameters and the friction velocity are shown in Figures 4.14, 4.15 and 4.16.

Figure 4.14 indicates an approximately constant momentum thickness error. This error is believed to be due to the error in the prediction of the boundary layer thickness, since the behavior of the momentum thickness is captured. Therefore it is thought that it will be removed with the correct prediction of the boundary layer thickness.

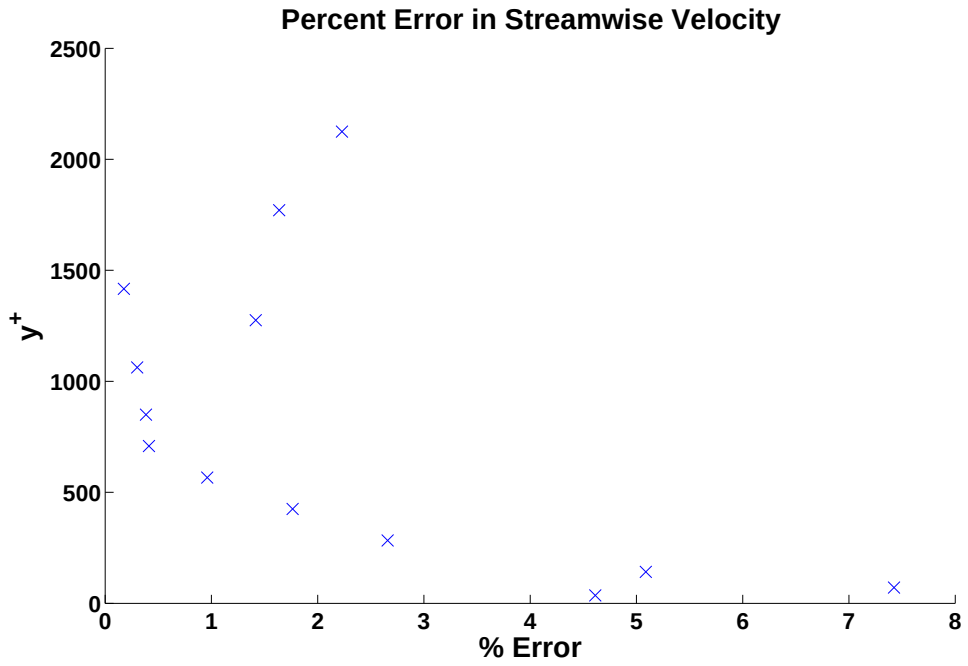

Figure 4.13: Percent error with the experimentally measured and computed velocity profiles for Favorable Pressure Boundary Layer for for $x = 4.085m$

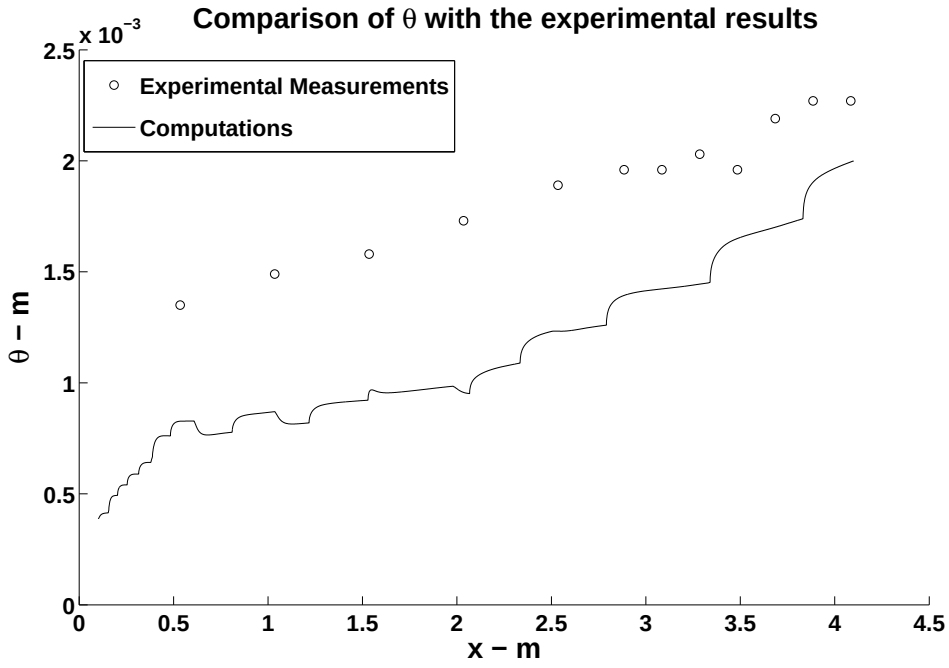

Figure 4.14: Comparison of experimentally measured and computed momentum thicknesses for Favorable Pressure Boundary Layer

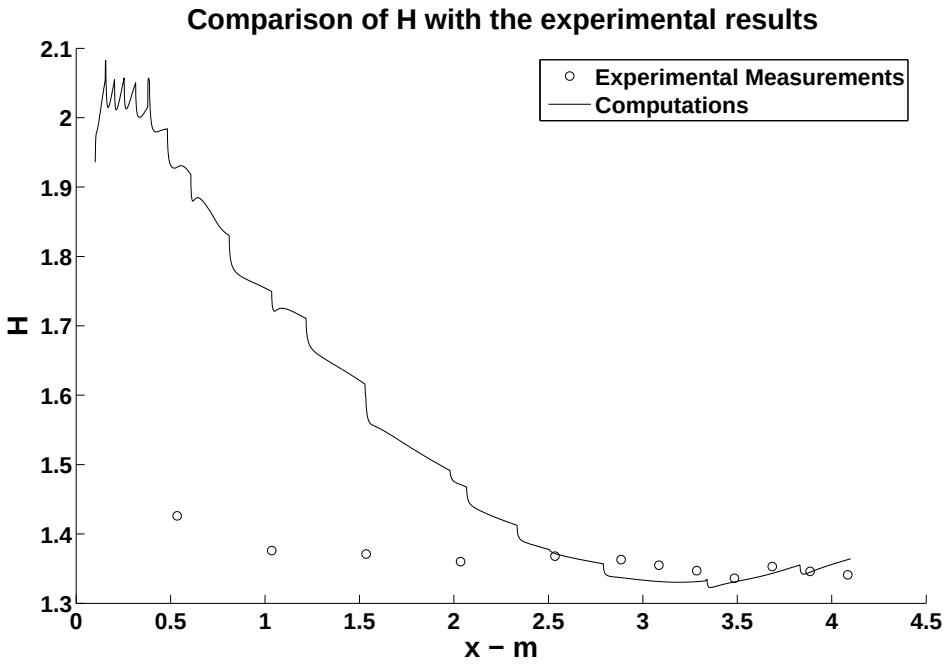

Figure 4.15: Comparison of experimentally measured and computed shape factors for Favorable Pressure Boundary Layer

Figure 4.15 indicates a decreasing error in the shape factor. As the trailing edge is approached, the error decreases to approximately zero value. The initial error in the shape factor (on the order of 40%) is believed to be due to the artificial initial condition of the flow and it is believed that it will reduce if appropriate initial conditions are used.

Figure 4.16 indicates a surprisingly accurate prediction for the friction velocity, especially near the trailing edge, compared to the errors present in the integral parameters. It can be argued that the 20% error at the leading edge is due to the error in the shape factor, hence due to the artificial initial condition of the flow. With the improvements in the shape factor predictions, it is believed that this error level will be reduced.

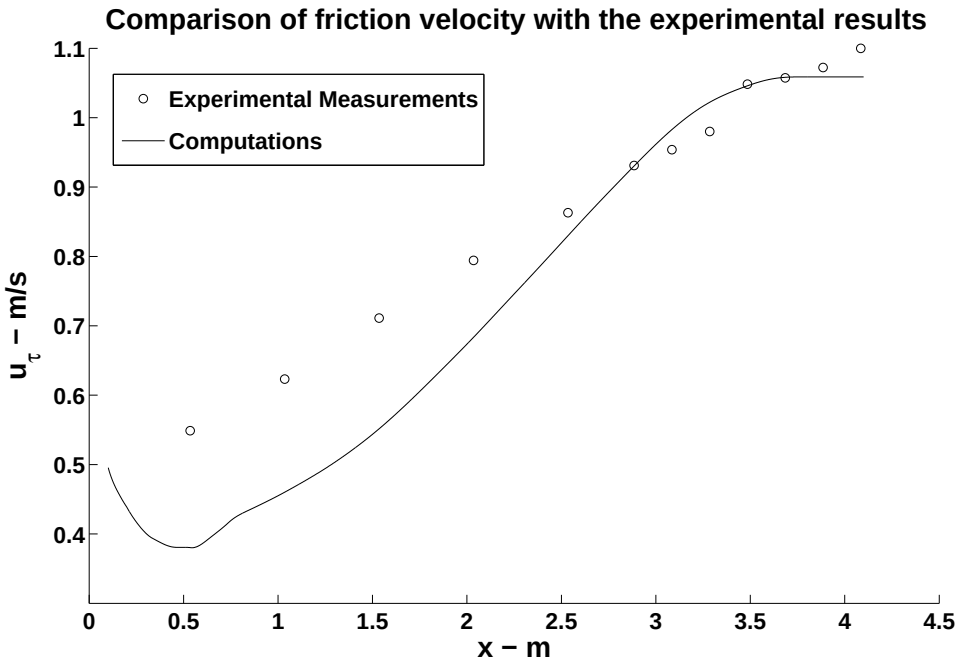

Figure 4.16: Comparison of experimentally measured and computed friction velocity for Favorable Pressure Boundary Layer

4.3 Solution over a Flat Plate with Adverse Pressure Gradient

The boundary layer flows under adverse pressure gradient is one of the difficult cases for turbulence models to predict. In order to test the New Model under this condition, experimental data from [1] is used (TBL10 test case). The flow conditions are given in Table 4.4.

Table 4.4: The experimental conditions for the flat plate with adverse pressure gradient

U_∞ (m/s)	ρ (kg/m^3)	ν (m^2/s)
10.38	1.225	$1.54 \cdot 10^{-5}$

The experimentally measured c_p and the one used in the calculations is shown in Figure 4.17. As can be seen from Figure 4.17, piecewise linear fit is applied to

the experimentally measured c_p to avoid the error in the calculation of derivative of c_p.

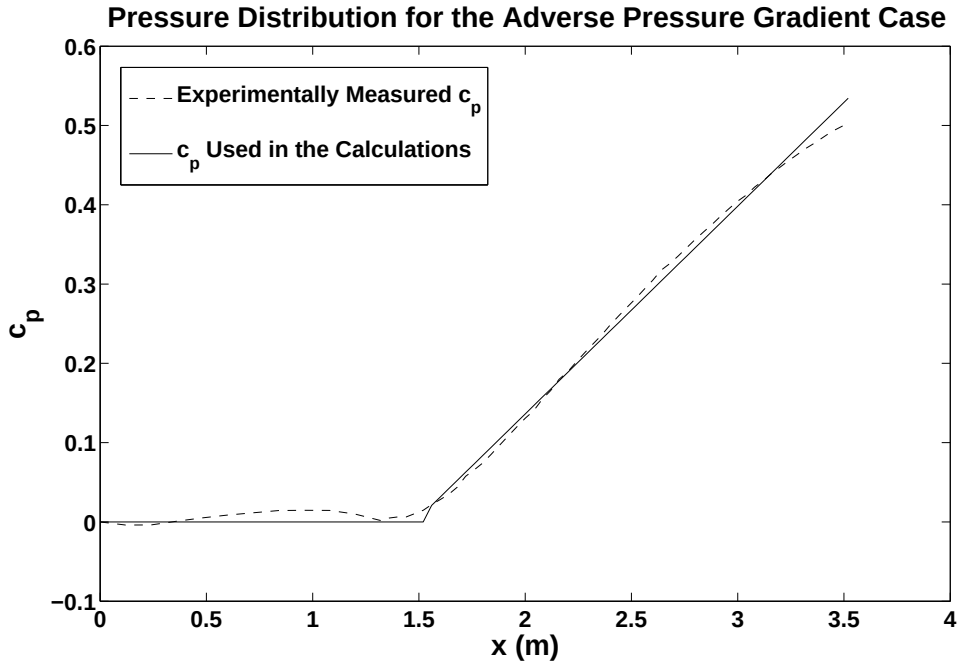

Figure 4.17: Pressure distribution for adverse pressure gradient case

The comparison will be made in two points; at $x = 1.2m$ and at $x = 2.88m$. The results are shown in Figures 4.18, 4.19, 4.20, 4.21.

The comparison of integral parameters are given in Table 4.5.

Table 4.5: The comparison of experimental data for the flat plate with adverse pressure gradient with computations

	x (mm)	u_τ (m/s)	δ (mm)	Re_θ	H
Experimental Measurement	1.2	1.18	27.72	2206	1.43
Calculation	1.2	0.27	8.98	266	2.06
Experimental Measurement	2.88	0.67	75	7257	1.73
Calculation	2.88	0.35	59	293.78	1.48

Unfortunately, results for adverse pressure case is not very promising. An error in the order of 70% is present. This seems the lack of turbulence model to

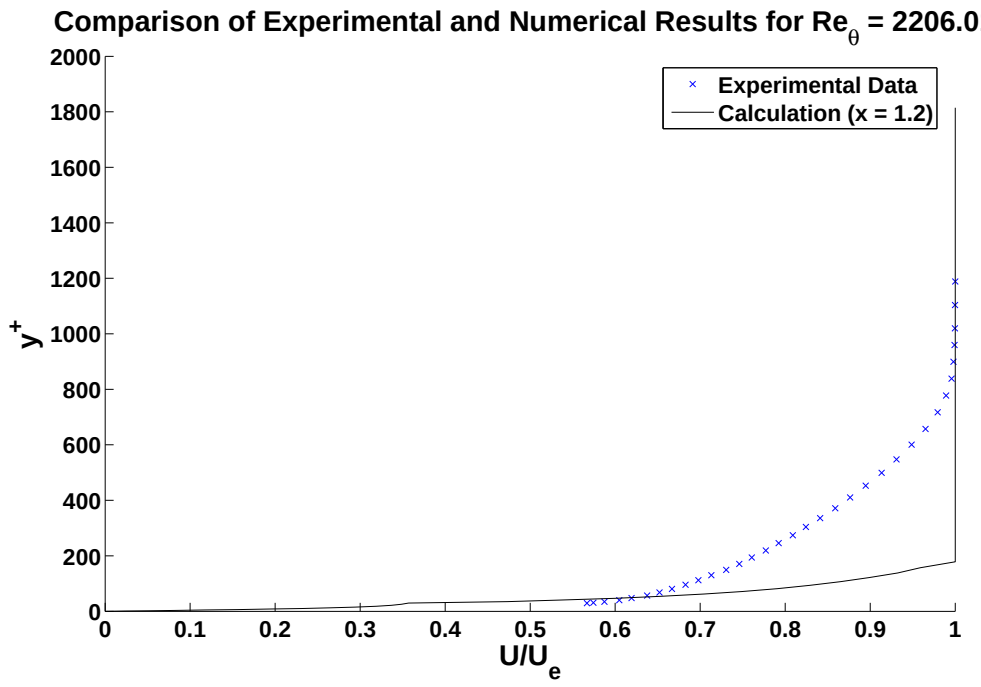

Figure 4.18: Comparison of experimentally measured and computed velocity profiles for Adverse Pressure Boundary Layer for $x = 1.2m$

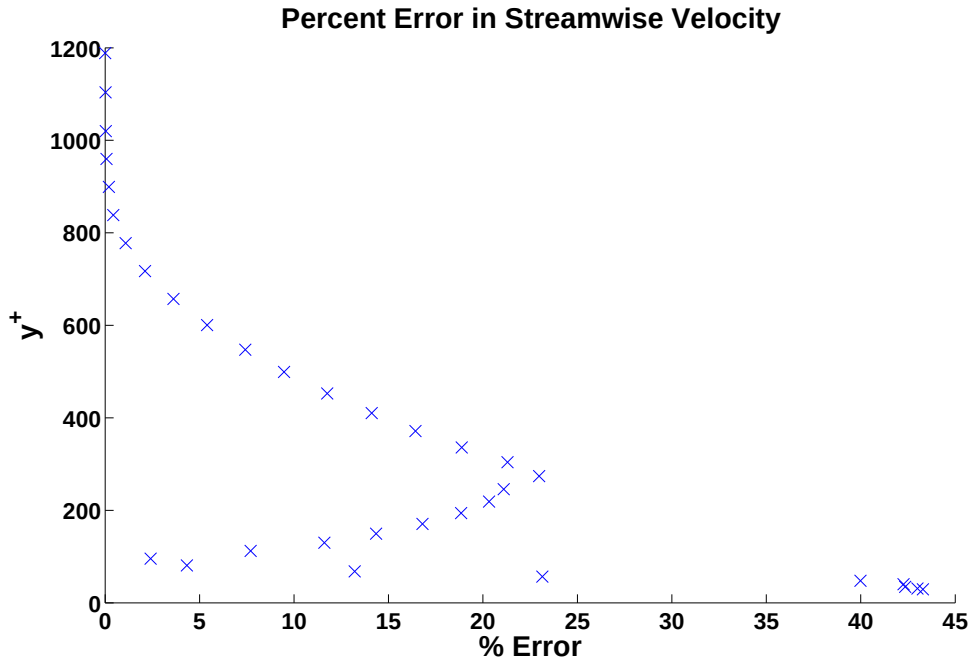

Figure 4.19: Percent error with the experimentally measured and computed velocity profiles for Adverse Pressure Boundary Layer for for $x = 1.2m$

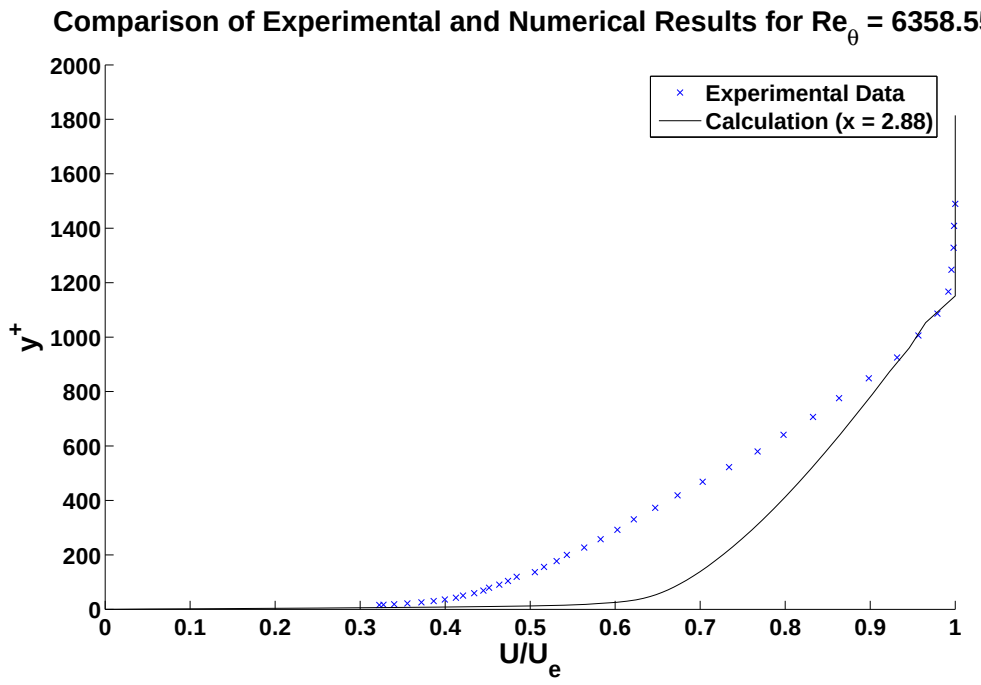

Figure 4.20: Comparison of experimentally measured and computed velocity profiles for Adverse Pressure Boundary Layer for $x = 2.88m$

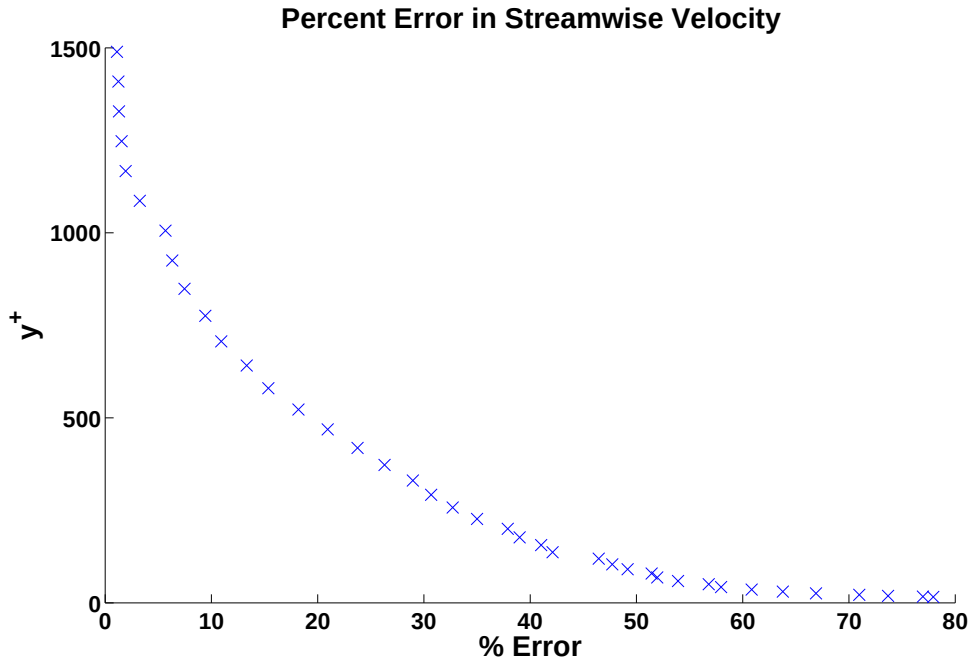

Figure 4.21: Percent error with the experimentally measured and computed velocity profiles for Adverse Pressure Boundary Layer for for $x = 2.88m$

represent the flows under adverse pressure gradient. However this is not exactly true. As can be seen from Table 4.5 that the momentum thickness is calculated very erroneously. This low value of momentum thickness affects the friction velocity and results in under-prediction of skin friction. This degrades the turbulence calculations in turn, since the New Model is proportional to the square of the skin friction velocity . If this feedback is cut, the performance of the predictions will increase. Actually better results can be achieved if flat plate correlations are used in u_τ and δ calculations which are shown in Figures 4.22 and 4.23.

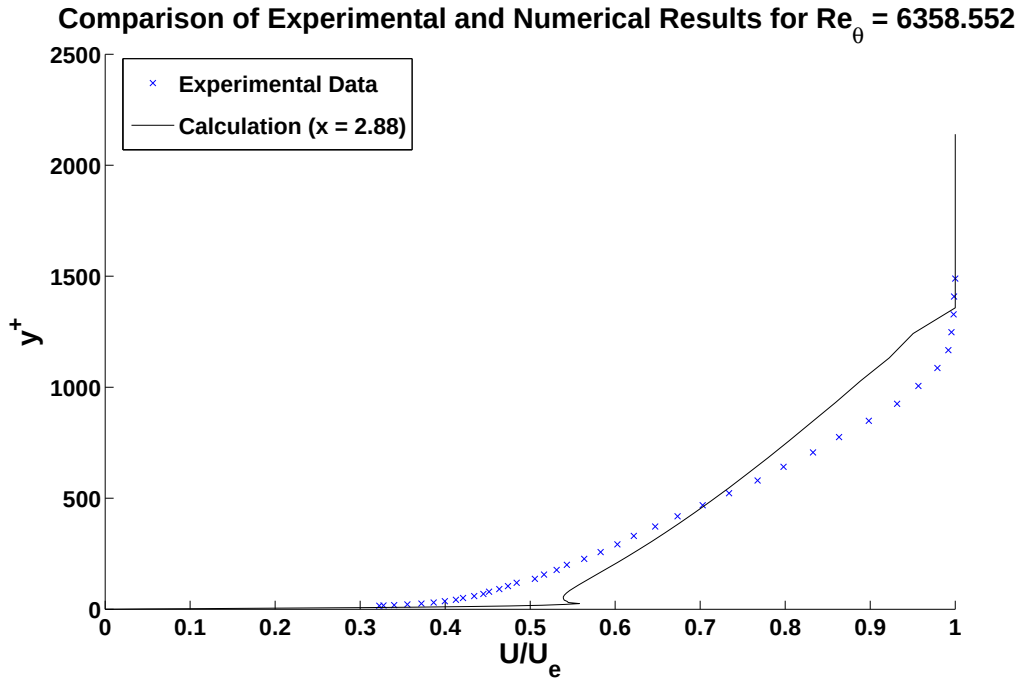

Figure 4.22: Comparison of experimentally measured and computed velocity profiles for Adverse Pressure Boundary Layer for $x = 2.88m$ (Flat Plate correlations are used for u_τ and δ)

The error is still seems as 70% but Figures 4.21 and 4.23 have a very important difference. The error shown in Figure 4.23 is accumulated in the near wall region. Therefore it is due to the near wall treatment. The error decreases rapidly to 20 %

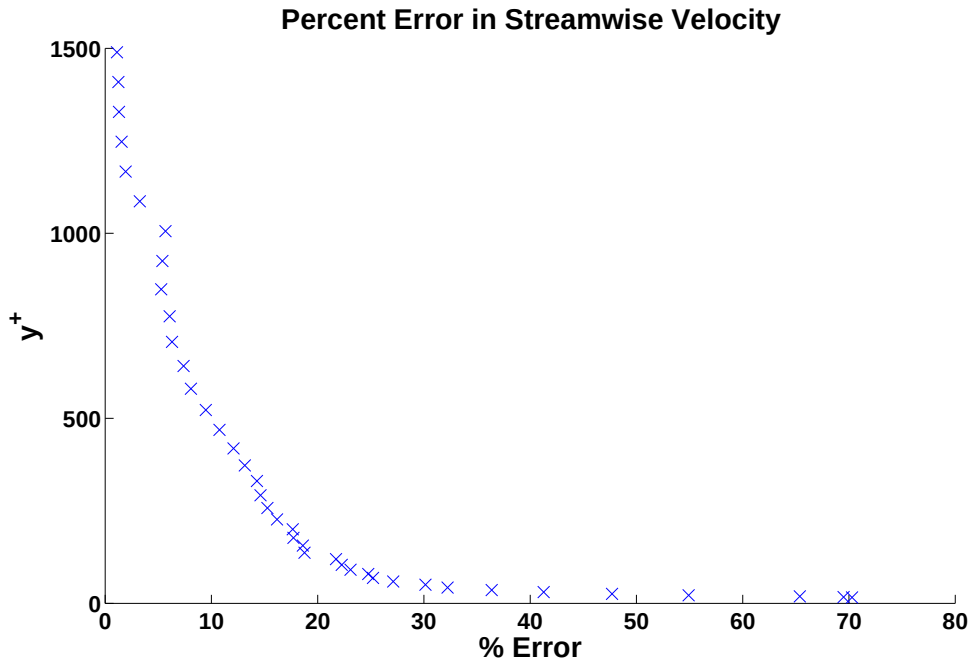

Figure 4.23: Percent error with the experimentally measured and computed velocity profiles for Adverse Pressure Boundary Layer for for $x = 2.88m$ (Flat Plate correlations are used for u_τ and δ)

level, which is believed to be the actual performance of the New Model. Therefore it can be argued that erroneous solutions for the adverse pressure gradient case is not due to the New Model's predictions, but is mainly due to the handling of the code to calculate skin friction and boundary layer thickness.

CHAPTER 5

DISCUSSION

In this thesis work, a new turbulence model is evaluated for boundary layer flows with and without pressure gradient. For this purpose, a boundary layer solver is developed.

The working principles of the code is explained in Chapter 3 and the performance of the model is evaluated in Chapter 4. In this chapter, some issues about the solver and the turbulence will be discussed.

5.1 The Boundary Layer Solver

The developed boundary layer solver is developed for the solution of the flows on flat plates. It uses boundary layer equations as the main flow equation. Von Karman momentum integral equation is used to find the skin friction. Boundary layer thickness is found within the solution procedure. Therefore there is no need to an external experimental/numerical results. General flow conditions like freestream velocity, density etc. is sufficient in order to solve the flow. It can be

used with virtually any turbulence model. But the issues that will be mentioned below should be taken with care.

- The errors in calculations mostly due to the handling of the momentum integral equation. Various fitting and smoothing techniques are used in the calculations and it can not be claimed that the procedure can be applied to solution of any flow. Care must be taken for this point when generating solutions.

- The solver is developed for turbulent flows but it can be applied to laminar flows also. Turbulent shear stress should be taken as zero and the wall correction to the streamwise velocity should be removed. The initial velocity profile generation should be replaced with the laminar case.

- The solver is developed for flat plate flows but it can be used with fully developed channel flows as well. For this purpose, the boundary layer thickness should be taken as the half height of the channel and the initial velocity profile generation should be adjusted.

- When integrating another model to the solver, it should be kept in mind that solver is specifically developed for the new turbulence model explained in this thesis. Therefore there might be modifications within the general solution procedure to overcome the difficulties with the new model, like the velocity correction near the wall. These modifications should be removed before integration.

5.2 The New Turbulence Model

It is shown in Chapter 4 that the model is suitable to be used in turbulent flow calculations. Its algebraic structure makes it free from numerical difficulties and decreases the computation time. However its current state is not mature enough to be used for industrial purposes.

Like many other turbulence models, the model has a difficulty in modelling the behavior of the turbulence near the wall (roughly, $y^+ < 50$). The further research should be focused on this region through finding appropriate wall functions. With the correct representation of the wall region, it can be implemented in a RANS solver. For the implementation into a RANS solver, it should be kept in mind that model requires a prior knowledge about the flowfield, namely the friction velocity u_τ and the boundary layer thickness δ. The correct representation of these parameters are essential for the model. Flat plate correlations can be used as an initial guess or the turbulence calculations can be started after some iterations are conducted. However this will result in starting the solution from laminar solutions. Since laminar friction velocity is smaller than turbulent one in general, the models shear stress prediction will be smaller than the actual solution. Therefore it is thought that such an approach will slow down the convergence rate. Hence it is advised to use flat plate correlations as the initial guess.

As discussed in Chapter 4, the errors in the results that are presented in this thesis are mainly due to the erroneous calculation of the friction velocity. Therefore it is thought that the performance of the model will be higher when

implemented in a RANS solver.

The future research on the model should be in the direction of finding appropriate wall functions and further validation of the model in more complex cases such as boundary layer flows under variable pressure gradient (like flow around an airfoil), separated boundary layers etc.

REFERENCES

[1] AGARD, "*A Selection of Test Cases for the Validation of Large-Eddy Simulations of Turbulent Flows*," Technical Report AGARD-AR-345 (NATO), 1998.

[2] Anderson, J. D. Jr., "*Fundamentals of Aerodynamics,*" 2nd Ed., McGraw-Hill Inc., 1991

[3] Asma, C. O., "*A Study into Isovels of Channel Flows*," Master Thesis, METU, May 2000.

[4] Ascher, M., *Lecture Notes*, 2003

[5] Baldwin, B., Lomax, H., "*Thin-Layer Approximation and Algebraic Model for Separated Turbulent Flows,*" AIAA 16th Aerospace Sciences Meeting, Huntsville, 1978.

[6] Bendat, J. S., Piersol A. G., "*Random Data : Analysis and Measurement Procedures,*" John Wiley & Sons Inc., 1971

[7] Bender, C. M., Orszag., S. A., "*Advanced Mathematical Methods for Scientists and Engineers,*" McGraw-Hill Inc., New York, 1978

[8] Boreé, J., *Lecture Notes for* AE701 Turbulence *Course*, 2004

[9] Bradshaw, P. (Editor), "*Turbulence,*" 2nd Ed., Springer-Verlag Berlin Heidelberg, New York, 1978

[10] Buschmann, M. H., Gad-el-Hak M., "*Debate Concerning The Mean-Velocity Profile of a Turbulent Boundary Layer,*" AIAA Journal, Vol. 41, No. 4, April 2003, pp. 565-572.

[11] Coles D.E., Hirst, E. A., "*Computation of Turbulent Boundary Layers-1968 AFOSR -IFP-Stanford Conference,*" Vol. II, Stanford University, 1968

[12] George, W. K., Castillo, L., "*Boundary Layers with Pressure Gradient: Another Look at The Equilibrium Boundary Layer,*" In R. M. C. So, C. G. Speziale, and B. E. Launder, editors, *Near Wall Turbulent Flows*, pp. 901-910. Elsevier, NY, 1993.

[13] George, W. K., Castillo, L., "*The Zero Pressure Gradient Turbulent Boundary Layer,*" Applied Mech. Rev., 50(12), 1997, pp. 689-729.

[14] Hoffmann, K. A., Chiang , S. T., "*Computational Fluid Dynamics for Engineers,*" Enginnering Education System, 1993

[15] Ilinca, F., Pelletier, D., "*Positivity Preservation and Adaptive Solution of Two-Equation Models of Turbulence,*" Int. J. Therm. Sci., 38, 1999, pp. 560-571.

[16] Kilerci, S., "*A Trial for New Turbulence Model for Low Reynolds Number Turbulent Boundary Layers*," Master Thesis, METU, January 2000.

[17] Kreyszig, E., "*Advanced Engineering Mathematics,*" 8th Ed., John Wiley & Sons Inc., 1999

[18] Lancaster, P., Salkauskas, K., "*Curve and Surface Fitting : An Introduction,*" Academic Press, 1986.

[19] Menter, F. R., "*Influence of Freestream Values on $k-\omega$ Turbulence Model Predictions,*" AIAA Journal, Vol. 30, No. 6, 1992, pp. 1657-1659.

[20] Menter, F. R., "*Two-Equation Eddy-Viscousity Turbulence Models for Engineering Applications,*" AIAA Journal, Vol. 32, No. 8, August 1994, pp. 1598-1605.

[21] Palliam, T. H., "*Euler and Thin Layer Navier-Stokes Codes : ARC2D, ARC3D,*" Notes for Computational Fluid Dynamics User's Workshop, Tennessee, 1984

[22] Pope, S. B., "*Turbulent flows,*" Cambridge University Press, Cambridge, 2000.

[23] Sarkar, A., So, M. C., "*A Critical Evaluation of Near-Wall Two-Equation Turbulence Models Against Direct Numerical Simulation Data,*" Int. J. Heat and Fluid Flow, Vol. 18, No. 2, April 1997, pp. 197-208.

[24] Schlichting, H., "*Boundary Layer Theory,*" 7th Ed., McGraw-Hill Inc., 1979

[25] Thompson J. F., Warsi Z. U. A., Mastin C. W., "*Numerical Grid Generation: Foundations and Applications,*". North-Holland, 1985

[26] Thivet, F., Daouk M., Knight, D. D., "*Influence of The Wall Condition on $k-\omega$ Turbulence Model Predictions,*" AIAA Journal, Vol. 40, No. 1, 2002, pp. 179-181.

[27] Townsend, A. B., "*The Structure of Turbulent Shear Flow,*" Cambridge University Press, Cambridge, 1956.

[28] White, F. M., "*Viscous Fluid Flow,*" 2nd Ed., McGraw-Hill Inc., 1991

[29] Wilcox, D. C., "*Comparison of Two-Equation Turbulence Models for Boundary Layers with Pressure Gradient,*" AIAA Journal, Vol. 31, No. 8, August 1993, pp. 1414-1421.

[30] Wilcox, D. C., "*Turbulence Modeling for CFD,*" DCW Industries Inc., California, 1994.

APPENDIX A

A General Cubic Spline Fitting Formulation

Spline fitting is a very commonly used technique in many different applications like interpolation, grid generation etc. In this work, it is used whenever two functions should be smoothly connected within an interval. Cubic polynomials are used as spline function since they permit the smoothness in first and second derivatives. But the calculation of the spline function for different functions results in derivation of formulation repeatedly. To avoid this, a single formulation is derived by transforming the fitting interval into another domain. The derivation is actually, application of more general technique, usage of *Cardinal Functions*, used in general spline fitting formulations ([18]).

Let $x \in \Re$ be the domain where functions f_1 and f_2 are defined and it is desired that functions $f_1(x)$ and $f_2(x)$ will be connected within the interval $[x_1, x_2]$. $f_1(x)$ is valid for $x \leq x_1$ and $f_2(x)$ is valid for $x \geq x_2$.

In order to connect $f_1(x)$ and $f_2(x)$, a transformation is defined for $x \rightarrow \eta$ where $\eta \in [0, 1]$ as,

$$\eta = \frac{x - x_1}{x_2 - x_1} \tag{A.1}$$

A cubic polynomial can be defined as,

$$F(\eta) = a_3 \cdot \eta^3 + a_2 \cdot \eta^2 + a_1 \cdot \eta + a_0$$

It is derivative can easily calculated as,

$$F' = \frac{dF}{d\eta} = 3 \cdot a_3 \cdot \eta^2 + 2 \cdot a_2 \cdot \eta + 1$$

In order to calculate the four coefficients (a_0, a_1, a_3, a_3), F and F' should be written at two points, η_0 and η_1 which results in system of four equations, given in (A.2)

$$\begin{bmatrix} 1 & \eta_0 & \eta_0^2 & \eta_0^3 \\ 0 & 1 & 2 \cdot \eta_0 & 3 \cdot \eta_0^2 \\ 1 & \eta_1 & \eta_1^2 & \eta_1^3 \\ 0 & 1 & 2 \cdot \eta_1 & 3 \cdot \eta_1^2 \end{bmatrix} \cdot \begin{bmatrix} a_0 \\ a_1 \\ a_2 \\ a_3 \end{bmatrix} = \begin{bmatrix} F|_{\eta=\eta_0} \\ F'|_{\eta=\eta_0} \\ F|_{\eta=\eta_1} \\ F'|_{\eta=\eta_1} \end{bmatrix} \tag{A.2}$$

For $\eta_0 = 0$ ($x = x_1$), $\eta_1 = 1$ ($x = x_2$), (A.2) becomes :

$$\begin{bmatrix} 1 & 0 & 0 & 0 \\ 0 & 1 & 0 & 0 \\ 1 & 1 & 1 & 1 \\ 0 & 1 & 2 & 3 \end{bmatrix} \cdot \begin{bmatrix} a_0 \\ a_1 \\ a_2 \\ a_3 \end{bmatrix} = \begin{bmatrix} F(0) \\ F'(0) \\ F(1) \\ F'(1) \end{bmatrix}$$

or

$$\begin{bmatrix} a_0 \\ a_1 \\ a_2 \\ a_3 \end{bmatrix} = \begin{bmatrix} 1 & 0 & 0 & 0 \\ 0 & 1 & 0 & 0 \\ 1 & 1 & 1 & 1 \\ 0 & 1 & 2 & 3 \end{bmatrix}^{-1} \cdot \begin{bmatrix} F(0) \\ F'(0) \\ F(1) \\ F'(1) \end{bmatrix} \tag{A.3}$$

In order to evaluate (A.3), values for $F(0)$, $F'(0)$, $F(1)$ and $F'(1)$ should be determined. But they can be calculated from f_1 and f_2 as,

$$\begin{aligned} F|_{\eta=0} &= f_1|_{x=x_1} \\ \left.\frac{\partial F}{\partial \eta}\right|_{\eta=0} &= \frac{\partial x}{\partial \eta} \cdot \left.\frac{\partial f_1}{\partial x}\right|_{x=x_1} \\ F|_{\eta=1} &= f_2|_{x=x_2} \\ \left.\frac{\partial F}{\partial \eta}\right|_{\eta=1} &= \frac{\partial x}{\partial \eta} \cdot \left.\frac{\partial f_2}{\partial x}\right|_{x=x_2} \end{aligned}$$

$\frac{\partial x}{\partial \eta}$ can be calculated directly from (A.1) as,

$$\frac{\partial x}{\partial \eta} = x_2 - x_1$$

Finally, (A.3) can be written as ,

$$\begin{bmatrix} a_0 \\ a_1 \\ a_2 \\ a_3 \end{bmatrix} = \begin{bmatrix} 1 & 0 & 0 & 0 \\ 0 & 1 & 0 & 0 \\ -3 & -2 & 3 & -1 \\ 2 & 1 & -2 & 1 \end{bmatrix} \cdot \begin{bmatrix} f_1|_{x=x_1} \\ (x_2 - x_1) \cdot \left.\frac{\partial f_1}{\partial x}\right|_{x=x_1} \\ f_2|_{x=x_2} \\ (x_2 - x_1) \cdot \left.\frac{\partial f_2}{\partial x}\right|_{x=x_2} \end{bmatrix} \tag{A.4}$$

Calculated a_0, a_1, a_3 and a_3 can be used to calculate $x \in [x_1, x_2]$ as,

$$f(x) = a_3 \cdot \left(\frac{x - x_1}{x_2 - x_1}\right)^3 + a_2 \cdot \left(\frac{x - x_1}{x_2 - x_1}\right)^2 + a_1 \cdot \left(\frac{x - x_1}{x_2 - x_1}\right) + a_0 \qquad \text{where} \qquad x \in [x_1, x_2]$$